MEASUREMENT OF BETA-RAY SPECTRA USING SCINTILLATION SPECTROMETER

by

Kuruvilla Verghese

A Thesis Submitted to the
Graduate Faculty in Partial Fulfillment of
The Requirements for the Degree of
MASTER OF SCIENCE

Major Subject: Nuclear Engineering

Iowa State University
Of Science and Technology
Ames, Iowa

1960

TABLE OF CONTENTS

I. INTRODUCTION

The scintillation spectrometer is rapidly gaining prominence as a powerful tool in nuclear studies. Its usefulness in measuring gamma ray spectra has already been established. But its application in measuring the energy spectra of beta rays has not been examined thoroughly. Measurement of beta ray spectra is important in nuclear physics mainly because of the fact that it leads us to the angular momentum and parity changes involved in the transition and the determination of these characteristics helps us to investigate the disintegration scheme. There is no classical theory for beta decay corresponding to the theories of electromagnetic radiation for gamma rays. The details we can obtain by studying the beta ray spectra bring to light a new type of interaction which is considerably more complicated than electromagnetic radiation.

Two distinctly different principles are used in the energy measurements of beta rays. One is based on the ionization produced by the beta particle in an absorbing medium when the particle is stopped in it. The other principle is to measure the momentum of the beta particle by deflecting it in a magnetic field. The first principle is utilized in scintillation spectrometry and the second one is made use of in magnetic-focusing spectrometers. The application of scintillation counter in beta ray spectroscopy fulfills the

need for a simple instrument capable of analyzing beta activities even though not with the precision of a magnetic spectrometer. The use of scintillation counter for this purpose has been investigated in the past only by using complicated, self-designed electronic circuits. It is worthwhile to examine the adaptability of a commercial equipment such as the Nuclear Chicago 1820 model spectrometer for this purpose and to show how precisely the shape of the spectrum can be obtained using such simple equipment.

In this type of work it is hard to say which scintillator will give the best results. Recently, a great deal of work has been done on organic scintillators and some of them have been proved to be very useful in detecting beta particles. The response of anthracene, stilbene and naphthalene to beta rays has been thoroughly studied. The pulse height produced in anthracene varies linearly with the energy of the impinging electron, its fluorescence decay time is of the order of 2×10^{-8} second and measurable pulses well above the background can be obtained even at electron energies as low as 10 to 12 Kev. Stilbene has even shorter fluorescence decay time, of the order of 8×10^{-9} second, but its conversion efficiency is only about half of that of anthracene. Naphthalene has a decay time of 8×10^{-8} second and its conversion efficiency is only about $\frac{1}{8}$ of that of anthracene. In view of these facts, it was decided to use anthracene and stilbene in this work.

Operation of the spectrometer for a wide range of beta ray end point energies was studied. Out of the several beta spectra measured, Cs^{137} had the lowest end point energy, 0.52 Mev and Rh^{106} had the highest, 3.53 Mev.

In Section III, a general description of the equipment used for measuring and recording the number of pulses for variation in energy will be given. Section IV deals with the methods of calculation used in the analysis of the spectra and in the determination of end point energies together with the corrections applied to the shape of the spectra. Section V is concerned with the experimental results obtained in the measurement of the spectra and with the calculation of end point energies.

II. REVIEW OF LITERATURE

The first simple form of the modern scintillation counter was introduced by Curran and Baker in 1944 (1). This was the first time a photomultiplier tube was used to deliver large pulses of current of short duration. At a later date, Kallman (2) discovered independently this method of radiation counting, and showed that both beta and gamma rays could be detected using single crystals of various luminescent materials to produce scintillations. Kallman's discovery of the possibility of using scintillation detectors to deduce the nature and energy of radiations from the pulse amplitudes was the first glimpse of a bright future for the scintillation counter in nuclear spectroscopy.

Almost at the same time, Coltman and Marshall (3) verified that the pulse height produced by a photomultiplier is directly proportional to the energy released in the phosphor. Kallman's observations were also confirmed and extended by Deutsch (4). Both of them used naphthalene for these studies and suggested anthracene as a possible alternative for such work. Bell (5) made a comparative study of naphthalene and anthracene and established the superiority of the latter in registering high pulses with a low background. For energy measurements of radiation, one has to know whether the number of light quanta emitted by the scintillator is actually proportional to the energy of the

radiation. This was shown to be so by Hopkins (6) with anthracene for monoenergetic electrons with energies above 125 Kev.

Shortly thereafter, many laboratories started investigations on the future of scintillation counter. Several ways to improve the quality of the photomultiplier were suggested by Morton (7) and also by Jordan and Bell (8) at a conference held at Oak Ridge in 1949. It was Bell (9) again, who showed that anthracene could be used effectively for beta-ray spectroscopy, in conjunction with suitable electronic circuits. Even today, Bell's work remains as a standard for scintillation counter studies of beta-ray spectra. He showed that the geometry of the instrument has appreciable influence on the shape of the spectrum obtained. The split crystal technique, suggested by Ketelle (10), has been shown by Bell to be the best geometrical arrangement.

Bell's work inspired Palmer and Laslett (11) to investigate the accuracy of beta spectra that can be obtained with a scintillation detector and a self-designed electronic circuit to analyze the pulses according to their energy. They showed that the determination of the end-point energies can be done with an accuracy of 8 percent or even better. It was their results that inspired this work.

A good deal of work has been conducted in determining the properties of various organic scintillators. The work of Sangster (12) is a valuable source of information on 27

purified organic crystals. He investigated the important properties of the phosphors such as emission spectra, transparency, wave length of emitted light, decay time, and conversion efficiency. He found that stilbene has considerably short decay time and relatively good response. The conversion efficiency of stilbene is almost half of that of anthracene, but the low value of its decay time makes this scintillator very valuable in high speed counting for which a minimum resolving time is required.

Anthracene, being the most widely used scintillator for electron counting, is known to be an ideal phosphor for beta work from the investigations of Bell (9) and of Palmer and Laslett (11).

Further survey of the literature in connection with this work will be given in later sections.

III. EXPERIMENTAL EQUIPMENT

A. The Scintillation Detecting Unit

This unit is a DS-5 model scintillation probe made by the Nuclear Chicago Corporation. It consists of the organic scintillator, a photomultiplier tube and a dual purpose preamplifier.

The anthracene and stilbene crystals used in this work were bought from the Crystals, Inc. The scintillator should be thick enough to stop all the beta particles impinging on it. In this work, the maximum beta ray energy was 3.53 Mev. The thickness of the crystal required to stop these high energy beta rays was calculated using the range-energy relationship for absorption of beta particles and $\frac{7}{8}$ inch thick crystals were obtained for this work. They were supplied in the canned form and the suppliers had to be relied upon for the quality of the crystals. It is obvious that the quality of the crystal determines to an appreciable extent the accuracy attainable in this kind of work. Each crystal is mounted in a cylindrical aluminum jacket with a very thin aluminum sheet at the front face which is exposed to radiation and a $\frac{1}{8}$ inch thick lucite light pipe at the other surface. It is sealed to the phototube with silicone grease. A cap which is screwed on to the phototube structure holds the crystal firmly in place with the help of two rubber washers and prevents outside light from entering the photo-

tube. The light from the scintillations is transmitted to the photocathode of the multiplier tube and an appreciable number of photoelectrons are emitted at the photocathode for each detected particle. Each one of these photoelectrons is drawn by an electrostatic potential to the first "dynode" where it ejects several secondary electrons. These electrons are in turn drawn to a second dynode and are similarly multiplied. In this manner, the multiplication is carried out in ten different stages and about half a million electrons appear at the anode of the photomultiplier tube, for each initial photoelectron.

The signal current pulses from the output of the photomultiplier pass through a 4.7 megohm coupling resistor in which proportional voltage pulses are developed to drive a preamplifier. The preamplifier consists of a 6BQ7A twin triode in a circuit designed to drive a scaler or a pulse height analyzer. A two position switch adapts the circuit to meet either requirement.

The phototube is sensitive to magnetic fields even as weak as that of the earth. A high permeability magnetic shield surrounds the photomultiplier tube to reduce the effect of external magnetic fields on the performance of the tube. Without magnetic shielding, the counting rate may change as much as 25 per cent for different orientations in the earth's field (11).

The photomultiplier-crystal assembly is held in a thick

lead shield which has two holders, one for the source and the other for absorbers, if they are needed.

In many experiments, it may be required to detect particles of low energy. The background noise in the photomultiplier determines this low energy limit. It has been proved experimentally that this noise could be reduced to a considerable extent by operating the photomultiplier tube at low temperatures (13). This work was done at room temperature and the background noise was found to be negligibly low down to energies as low as 15 to 20 Kev. Below this limit, there were several other predominating factors which contributed to excessive low energy pulses and so the background noise could be neglected for our purpose.

B. Radiation Analyzer

For the purpose of determining the true energy distribution and relative intensities of radiations, a Nuclear Chicago Model 1810 single-channel differential pulse height analyzer is provided in this spectrometer. A simplified block diagram of this Radiation Analyzer is shown schematically in Figure 1.

The voltage pulses from the scintillation detector are fed into the linear amplifier of this analyzer unit. These pulses are amplified to higher voltages depending on the constant gain of the amplifier. These amplified pulses are then fed into two amplitude-discriminating circuits, which we shall call the "base-level" discriminator and the "upper"

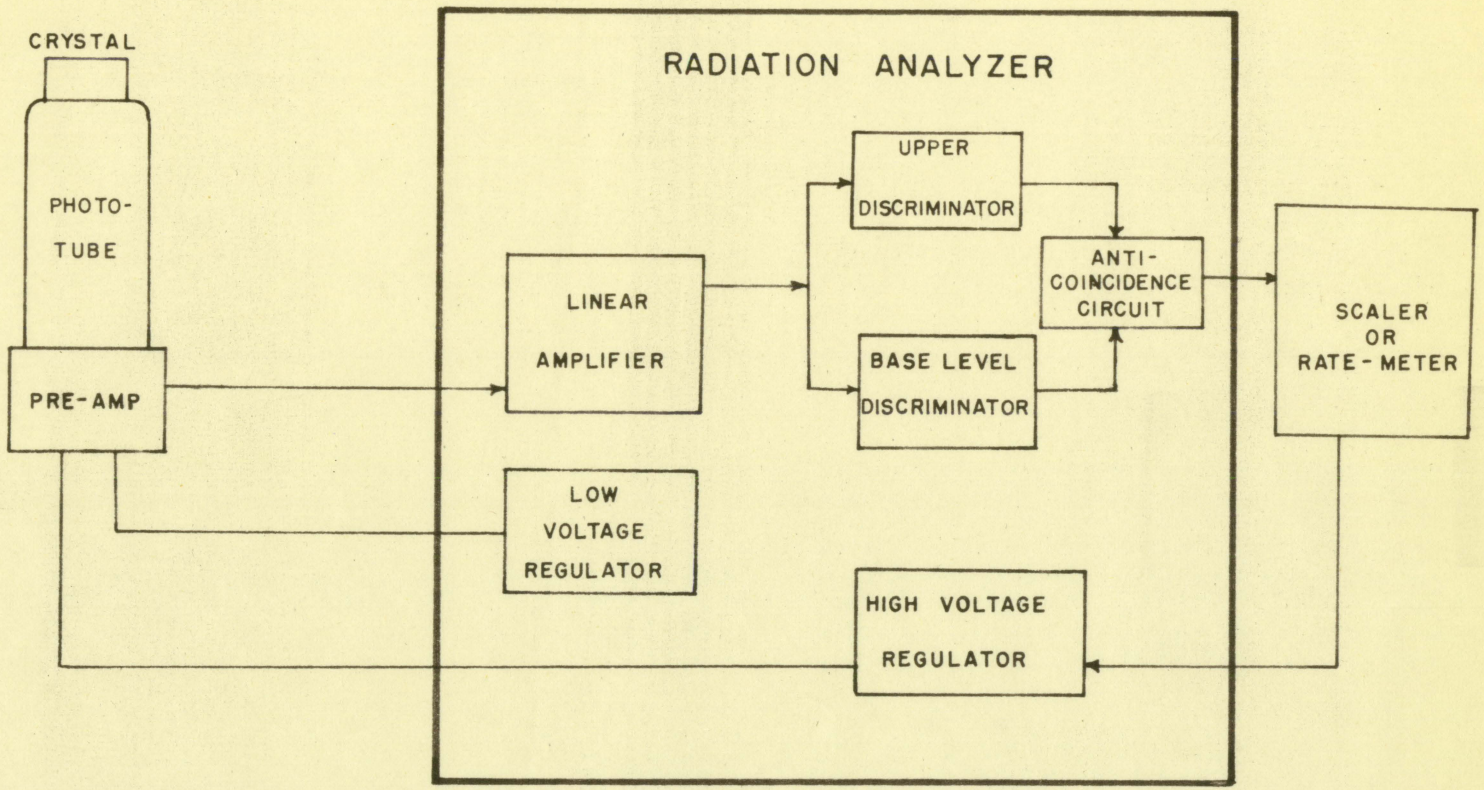

Figure 1. Simplified block diagram of the radiation analyzer

discriminator. The base-level discriminator may be varied in sensitivity from 1 to 100 volts. The preset voltage of this discriminator determines the voltage level below which all pulses it receives will be rejected. The control for the base-level discriminator is provided by a 10-turn potentiometer. The sensitivity of the upper discriminator may be varied by 10 volts with reference to the voltage of the base-level discriminator. This means that the voltage level below which all pulses will be rejected by the upper discriminator is determined by the sum of the preset voltages of the two discriminators or by $V_{base} + V_{upper}$. The control for the upper discriminator is provided by a single turn potentiometer which is called the voltage "window". The width of the voltage window is independent of the voltage setting of the base-level discriminator.

Both the discriminators feed into an "anticoincidence" circuit. For the purpose of illustrating how anticoincidence is obtained by the analyzer, we shall assume that the discriminator voltage settings are E_1 for the base-level discriminator and ΔE for the window. Then all pulses below the voltage level E_1 will be rejected by both the discriminators and the pulses between the range E_1 and $E_1 + \Delta E$ will be rejected by the upper discriminator. But the latter pulses will trigger the base-level discriminator. Pulses above the voltage level $E_1 + \Delta E$ will trigger both the discriminators. These pulses are fed into the anticoincidence

circuit. This circuit will pass only those pulses which are received from the base-level discriminator when the upper discriminator is not triggered simultaneously. When driven by both the discriminators, the pulses cancel each other and so no output pulse is produced. Therefore, for the conditions assumed, only the output pulse initiated by a pulse between the voltage levels E_1 and $E_1 + \Delta E$ will be obtained from the anticoincidence circuit. Any pulse above $E_1 + \Delta E$ is cancelled out, where as one below E_1 is rejected by the discriminators. Therefore by making the range between E_1 and $E_1 + \Delta E$ as small as possible by proper adjustment of the base-level and the window, separate selection of particular energy levels can be made. Pulses from the anticoincidence circuit are refined through a "trigger" circuit before being fed out of the Radiation Analyzer.

For the operation of this single channel pulse height analyzer as a part of the recording spectrometer, scanning of the energy range of the radiation is achieved by a non-recurrent and approximately linear sweep of the base-level discriminator voltage through a range of 100 to 1 volt or less. This is done by a motor driving the base-level control at a constant speed.

The energy range to be scanned may be changed from an established calibration by factors of two using a "gain" selector that is provided. The gain of the linear amplifier in the radiation analyzer is constant. The gain selector

is an attenuator at the input of the amplifier and it determines the overall gain of the scintillation detecting unit and the amplifier system or conversely, the signal level coming out of the scintillation counter necessary to produce a given amplifier output signal. Thus the required gain of the scintillation detector is inversely proportional to the gain factor, for any given energy calibration of the base-level dial. That is, if for a particular calibration, the base-level voltage range of 1 to 100 volts represents 10 Kev to 1 Mev, a reduction in gain by a factor of 2 will make the range approximately 20 Kev to 2 Mev.

The best signal-to-noise ratio and energy resolution are obtained from a scintillation counter when it is operated at a low gain or with a minimum usable voltage applied to the photomultiplier tube. This condition is satisfied when the "gain" selector is set to 8 or 16. But in the work, the highest gain had to be used often, because of the wide energy range of the beta spectra of some of the sources studied.

C. Count-Rate Meter

The selected pulses emerging from the radiation analyzer unit are made uniform in height and width by the "trigger" circuit, but they occur at a random rate characteristic of nuclear disintegrations. These pulses are fed into a count-rate meter and from there to a strip-chart recorder which

records the variation in counting rate.

The main function of the count-rate unit is to provide a known and adjustable time interval over which the random rate of the pulses that come in is averaged. This interval is adjusted by changing the time constant of the circuit. With too short a time constant, the meter and the recorder currants fluctuate excessively, especially at low counting rates, making accurate measurement difficult. With too long a time constant, the meter and the recorder respond too slowly to the pulses and for fairly good accuracy, the scanning rate would have to be very slow. This circuit is provided with a choice of four time constants. With too long a time constant, the effect on a spectrogram recorded is a slight displacement of all recorded information along the time axis of the chart and a recorded counting rate less than the true average. Therefore the minimum usable time constant has to be selected when running a spectrogram.

D. Recorder

The output signal from the rate meter is a fluctuating d.c. voltage with an average value proportional to the number of pulses per minute. This signal is fed into the strip-chart recorder. This precision recorder employs rectilinear pen displacement on a calibrated strip-chart 11 inches wide. The overall mechanism is known as a "self-balancing d.c. potentiometer." In operation, the d.c. input signal is

compared to a standard d.c. voltage by means of a potentiometer. The difference between the input and the standard voltages is then converted to 60-cycle a.c. and amplified to drive a power amplifier. This energizes a control winding in a "balancing motor". The output of the motor is coupled to the balance arm of the potentiometer and to the recording pen. The direction of rotation of the motor depends on the phase relation between the amplified difference signal which is applied to the control winding and that of a reference winding energized by the power line. The rotation of the motor will always be to try to establish potentiometer balance and when the balance is reached, the difference between the input signal and the standard voltage becomes zero and so the balancing motor stops. In this manner the balance system functions continuously to follow any changes in the input level. The counting rate is indicated by the pen displacement and radiation energy is represented by the distance along the time axis of the paper chart.

IV. METHOD OF PROCEDURE

A. Calibration of the Spectrometer

The most widely adopted way to calibrate the spectrometer is by using the monoenergetic internal conversion lines of isotopes emitting gamma rays. In this work, the well-known 624 Kev internal conversion line of Cs^{137} was used. Assuming a straight line variation of energy with the base-level voltage, energy at any point on the abscissa of the recorded spectrogram could be found. This assumption of linear variation, as will be shown later in this work, is not quite true because the end points of the beta spectra of high energy isotopes like Y^{90}, Pr^{144}, Rh^{106}, etc., were found to differ appreciably from the more accurate values determined using magnetic spectrometers. A better method for calibration would have been to get two or three calibration points instead of one in the range of the maximum energy to be measured. This was not done in this work, mainly because of nonavailability of isotopes required to get these calibration points within the duration of this investigation.

The high voltage control of the analyzer can be calibrated to give the maximum counting rate on the conversion line when the base level is set at 624 minor divisions. Then each minor division on the base-level control represents 1 Kev. In this work, it was often found necessary to reduce the gain factors in order to accomodate the complete spectra

of high energy beta sources, within the maximum possible scan of the base-level control. The calibration of the high voltage was done at a gain factor of 4, using the Cs^{137} internal conversion line. So, for each change in gain, the point on the abscissa at which the peak of the conversion line occurred had to be noted in order to get the energy calibration of the abscissa for each gain factor.

Peak differential response occurs when the voltage sensitivity at the center of the window coincides with the energy peak of the internal conversion line. Since the window voltage is added to the base-level voltage, the absolute voltage sensitivity at the center of the window is a function of the window width as well as the base-level voltage. So whenever the window width had to be changed, it was necessary to readjust the high voltage slightly to retain the calibration. In this work, the window width used in most of the cases was 2 volts, but very rarely, in the case of some weak samples, it was necessary to increase it in order to get an appreciable counting rate.

B. Plotting the Beta Spectra

Almost all the sources used for this work were samples evaporated on aluminum foil of thickness $\frac{1}{4}$ mil, and covered with thin cellophane tape. The Nd^{147} and Ru^{106} - Rh^{106} sources were obtained from the Ames Laboratory and they were samples precipitated and dried on filter paper, backed up

with aluminum planchets and covered on top with mylar film.

In the experiment, the sample was placed at a constant distance of 2.5 cms from the crystal. The range selector is then set to the lowest range that will accomodate the peak counting rate in the spectrum. Then the base-level control is turned clockwise and set at the starting point which should be the tail end of the spectrum. Now the base-level and chart-drive switch is turned on and the recorder pen starts to record the increase in counting rate as the scan of the base-level begins. A complete scan of the base-level from 1000 to 1 minor divisions will take 30 minutes and the chart drive travels 15 inches during the scan. This scanning range is linear with respect to energy above the last 10 percent of the chart in the direction in which the spectrum is plotted. So in a base-level drive from 1000 to 1, the variation of energy along the scanning range is linear from 1000 to 100 minor divisions. Below 100, the variation from this linear curve may be as high as 30 percent.

Typical spectrograms recorded on the strip chart are shown in Figure 2 and Figure 8. In the case of certain isotopes like Cs^{137}, Rh^{106}, etc., gamma rays are emitted in conjunction with electrons. The organic scintillators interact with gamma rays mainly by the Compton process and these Compton electrons are also counted when the spectra of these isotopes are recorded. In order to eliminate the effect of these gamma rays from the plotted spectra, a sepa-

rate run of the spectrogram is made with the sources covered with aluminum absorbers which are just thick enough to absorb all the beta particles. These recordings are made for each of the isotopes with the same instrument settings which were used for plotting the overall beta spectra. Since the aluminum absorbers filter out all the beta particles, only the counts due to the gamma rays are recorded in the second run. Thus by subtracting these counts from the original overall spectrum, the pure beta spectrum can be obtained. This may not be a very accurate method when compared to the coincidence techniques, but it gives reasonably good results and is a very simple and quick method.

C. Fermi Plots

For the energy spectrum of any single group of beta rays the number of electrons in a range dW of total energy can be written as

$$N_{\pm}(W)\,dW = \frac{g^2}{2\pi^3}\,F(\mp Z,W)\,p\,W\,(W_o - W)^2\,dW\,\left[S_n(W)\right]. \quad (1)$$

Here, $F(\mp Z,W)$ = the Coulomb factor which essentially represents the density of beta particles at the nuclear radius relative to the density at infinity.

$S_n(W)$ = the shape factor for forbidden spectra.

W = the total energy of the electron in $m_o c^2$ units.

p = the momentum of the electron in $m_o c$ units, i.e., $= \sqrt{W^2 - 1}$

and g = the coupling constant.

Equation 1 can be rewritten as

$$\frac{N_{\pm}(W)}{F(\mp Z,W)\ p\ W\ S_n(W)} = \frac{g^2}{2\pi^3}\ (W_o - W)^2 \qquad (2)$$

or

$$\left[\frac{N_{\pm}(W)}{F(\mp Z,W)\ p\ W\ S_n(W)}\right]^{\frac{1}{2}} = K\ (W_o - W)\ , \qquad (3)$$

where K = a constant.

Therefore, a plot of $\left[\frac{N_{\pm}(W)}{F(Z,W)\ p\ W\ S_n}\right]^{\frac{1}{2}}$ vs. W should be a straight line. This plot is known as a Fermi or Kurie plot. The intercept of this line on the W axis will be W_o, the total disintegration energy in $m_o c^2$ units, from which the end point energy E of the spectrum may be determined using the relation,

$$E = (W - 1)\ 0.511\ \text{Mev}. \qquad (4)$$

For allowed spectra, $S_n = 1$, so that the ordinate of the Kurie plot for an allowed transition reduces to $\left[\frac{N(W)}{F(\mp Z,W)\ p\ W}\right]^{\frac{1}{2}}$. The shape factors used to correct the forbidden transitions will be discussed in Section V. If we set $C = (\frac{p}{W})F$, the ordinate becomes $\left[\frac{N(W)}{C\ W^2}\right]^{\frac{1}{2}}$ or $\frac{1}{W}\sqrt{\frac{N(W)}{C}}$. The C values for our purpose are taken from the tables of Fermi functions compiled by M. E. Rose and others (14).

If more than one beta ray group is emitted from a source, a Kurie plot of the overall combined spectrum will show noticeable shift from a straight line. It will start from W_o as a straight line and break upwards at some point,

indicating the existence of one or more low energy groups of beta rays. In such cases, the different components can be separated by the conventional method of graphical analysis, as will be shown later. Although this method is inferior to beta-gamma coincidence techniques, it provides reasonable accuracy if the original shape of the spectrum is free of excessive distortion due to backing and source thickness. However, graphical analysis becomes complicated and inaccurate when the low energy groups have highly forbidden shapes. For this work, coincidence work was not available and graphical analysis was the only choice.

D. Transmission Corrections to the End Points

The fraction of all monokinetic electrons leaving the source which is actually counted in the detector is called spectrometer transmission. The transmission corrections, frequently referred to in this work, are based on a method evolved by Palmer and Laslett (11). Owing to the fact that all electrons of the same energy do not produce voltage pulses of the same height, a monoenergetic electron line when recorded in the spectrometer will appear as a line of certain width. This width is a good measure of the resolution or the resolving power of the instrument. The internal conversion peak shown in Figure 7 is a monoenergetic electron line and so its width is proportional to the resolving power of the instrument. This line has the shape of a Gaussian

distribution. Palmer and Laslett approximated this shape by the best fitting triangle. They showed that the correction is proportional to the width at half-maximum or the so-called "half-width" of the triangle. With a theoretical approach involving certain assumptions, they obtained a curve of the correction factor for the observed counts against the ratio,

$$\frac{\left[\text{Voltage at the true end point}\right] - \left[\text{Voltage of the pulse at the point where correction is to be applied}\right]}{\text{The half-width of the conversion line in voltage units.}}$$

The curve increases in an inverse exponential manner.

The effectiveness of this correction, if applied in our case, will be discussed in Section V.

V. RESULTS

A. Phosphorus-32

This isotope is known to be a pure beta emitter with a "log ft." value of 7.9, which is a characteristic of first-forbidden transitions. However, the spectrum of P^{32} has been investigated by P. R. Bell (14), L. M. Langer and H. C. Price, Jr. (15) and many others and it has been established that the shape of the spectrum is of the allowed type.

The P^{32} spectrum as recorded on the strip chart using an anthracene crystal is shown in Figure 2. It was also recorded using stilbene crystal with a sample of different activity. This spectrum is shown in Figure 3. A Kurie plot of the spectrum is shown in Figure 4. The energy calibration of the base-level scale was done with the 624 Kev peak of the internal conversion line of Cs^{137}, shown in Figure 5. The calculations involved in getting the Kurie plot are tabulated in Table 1, as a sample of calculated results. The end point energy determination from the Kurie plot gave a value of 1.94 Mev which agrees with the accepted value of 1.72 Mev to 11 percent.

Since P^{32} has an allowed spectrum, the Kurie plot should have been a straight line. But instead, it is found to have a slight upward curvature at low energies. A slight error in calibration would not have affected the shape so much. Palmer and Laslett (11) and also P. R. Bell noticed this curvature.

Figure 2. Strip-chart recording of P^{32} spectrum

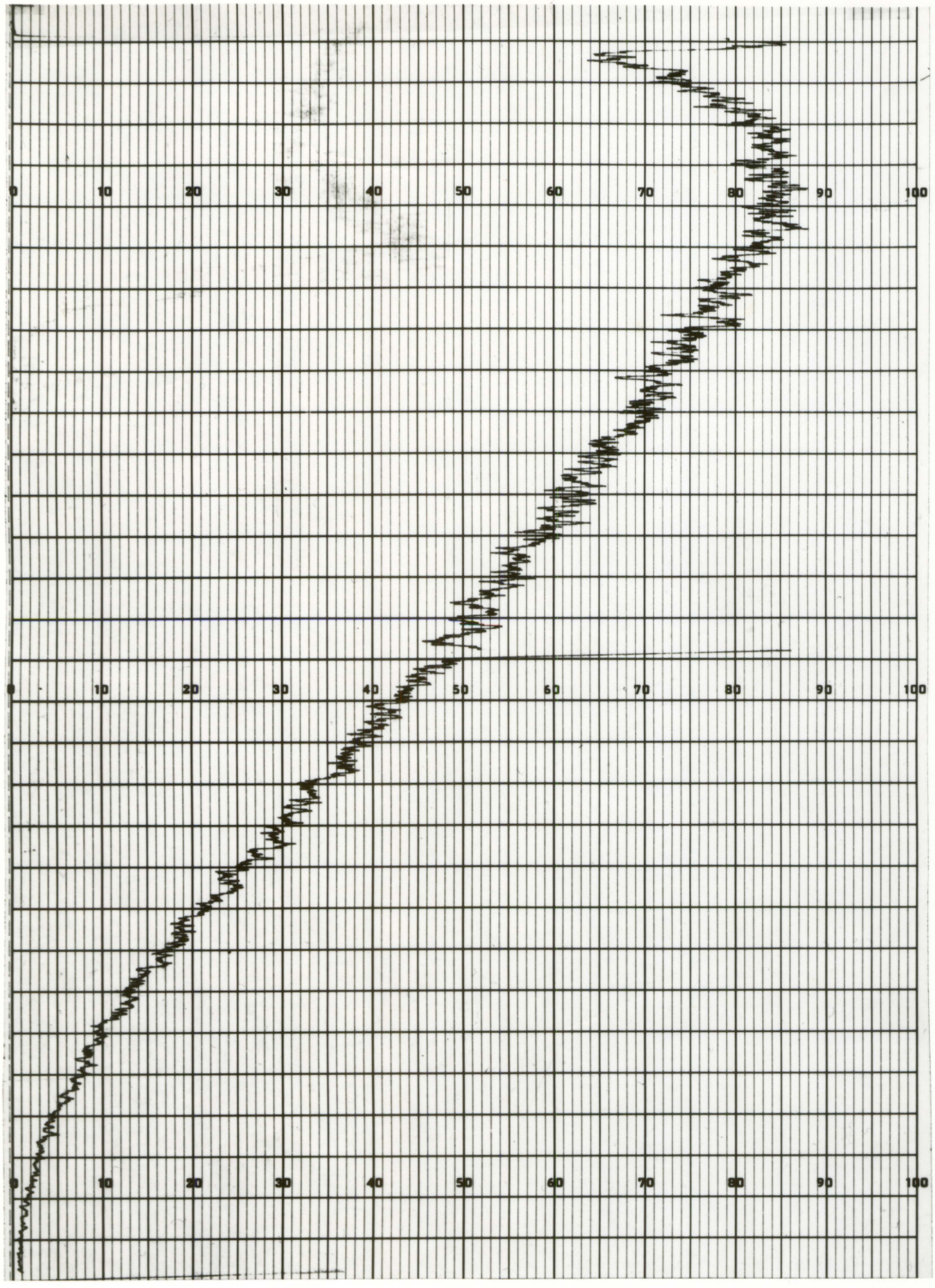
0
10
20
30
40
50
60
70
80
90
100

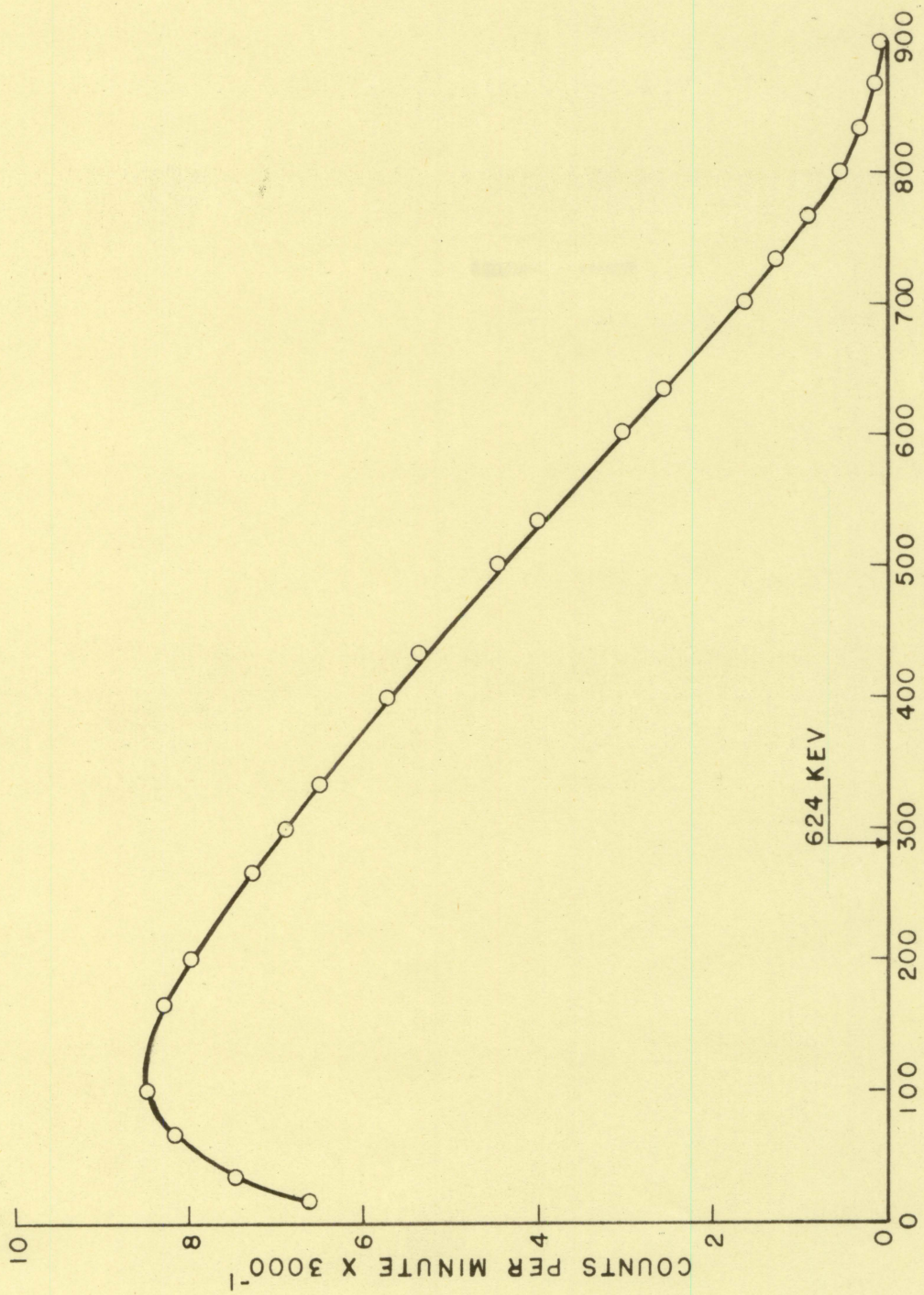

Figure 3. Experimental beta spectrum of P^{32}

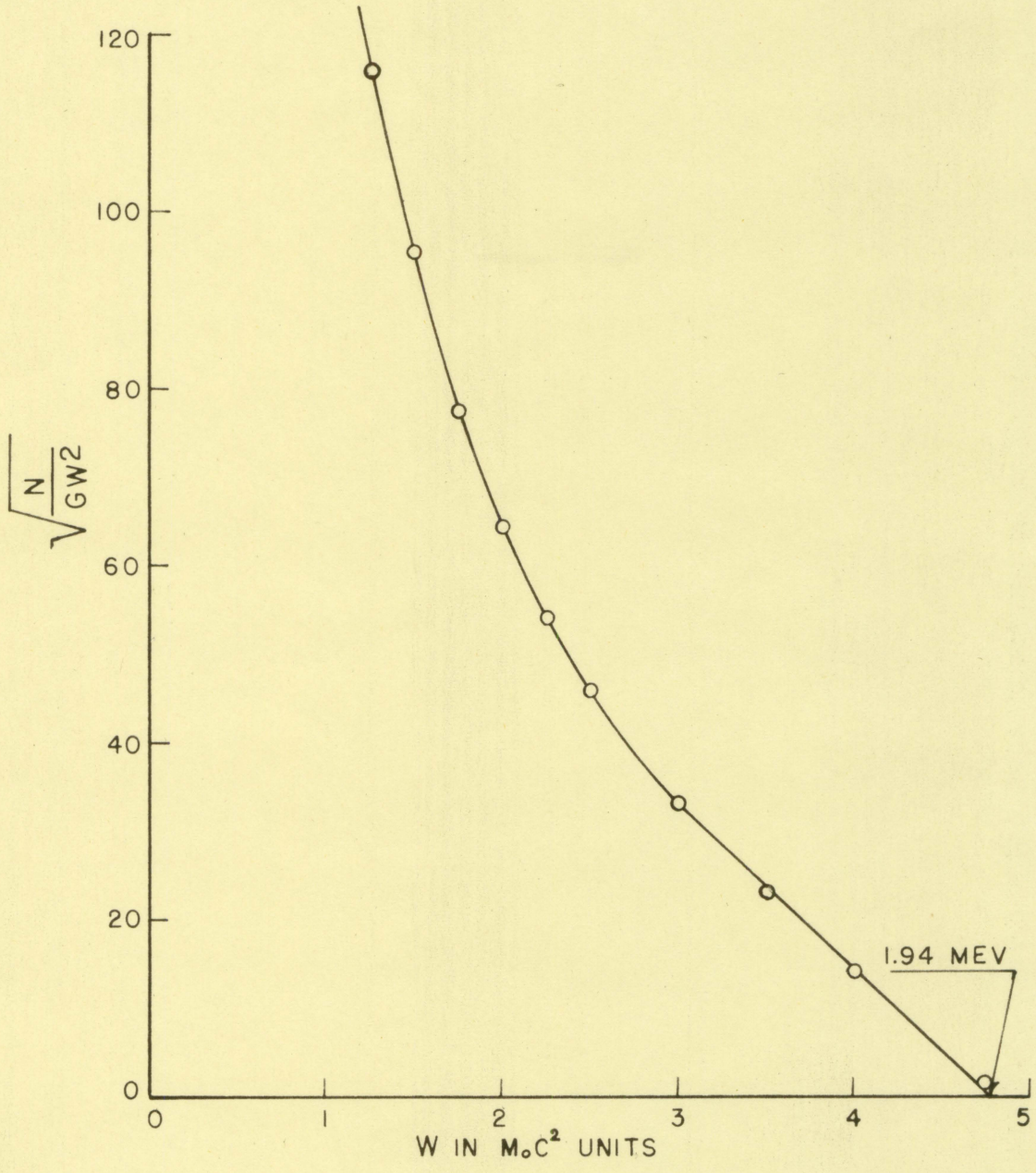

Figure 4. Kurie plot of the P^{32} spectrum

Table 1. Calculated data for the Kurie plot of P^{32} spectrum

Isotope: Phosphorus-32 Window width: 1.75 volts Range: 30,000
Scintillator: stilbene Time constant: 2 seconds Gain: 2

W (m_oc^2)	E (m_oc^2)	E (Mev)	Base level divisions	$\frac{N(W)}{k^a}$	p (m_oc)	G	$\frac{N}{aG}$	$\sqrt{\frac{N}{aG}}$	$\sqrt{\frac{N}{aGW^2}}$	$\frac{(\frac{N}{G})^{\frac{1}{2}}}{W}$
1.25	0.25	0.1278	59	78.8	0.7495	1.131	69.6	8.35	6.68	115.8
1.5	0.50	0.2555	118.5	85.0	1.118	1.241	68.5	8.27	5.51	95.5
1.75	0.75	0.3833	177.5	82.2	1.436	1.338	61.5	7.84	4.48	77.5
2.0	1.00	0.511	236	76.0	1.732	1.373	55.3	7.44	3.72	64.4
2.25	1.25	0.6388	296	69.9	2.016	1.408	49.7	7.05	3.13	54.2
2.5	1.50	0.7665	355	62.5	2.291	1.427	43.8	6.62	2.65	45.9
3.0	2.0	1.021	473	48	2.829	1.449	33.2	5.76	1.92	33.3
3.5	2.5	1.278	596	31.7	3.355	1.460	21.7	4.66	1.33	23.0
4.0	3.0	1.533	710	15.0	3.871	1.469	10.2	3.19	0.797	13.8
4.75	3.75	1.917	888	0.8	4.641	1.475	0.54	0.733	0.154	1.67

$^a k = 300$

This could have been due to the possibility that some of the electrons were scattered out of the crystal before they lost all of their energy in the crystal and so such pulses add to the true distribution at low energies. However, this error does not affect the end point.

This spectrum was plotted at a "Gain" factor of 2, at which the transmission corrections will make little effect on the spectrum, as will be shown later. So these corrections are not applied here.

B. Cesium-137

The radiations from this isotope are well known (16, 17). Its internal conversion peak at 624 Kev (18) was used for energy calibration in the case of all the spectra. So the Cs^{137} spectrum had to be recorded for all the "Gain" factors used in this work, Viz., 4, 2 and 1. The spectrum for a gain 2 and using the stilbene crystal is shown in Figure 5. The 624 Kev peak is found to be at 289 on the base-level scale. The same peak for gain equal to 4 and 1 were found to be at 624 and 138 respectively. For anthracene, these peaks were respectively at 624, 268, and 114 for gain 4, 2 and 1. These results are required for the energy calibration of other spectra.

In Figure 5, the "gross spectrum", the distribution due to gamma rays alone and the "gamma subtracted spectrum" are shown. Theoretically the pure beta-spectrum should come

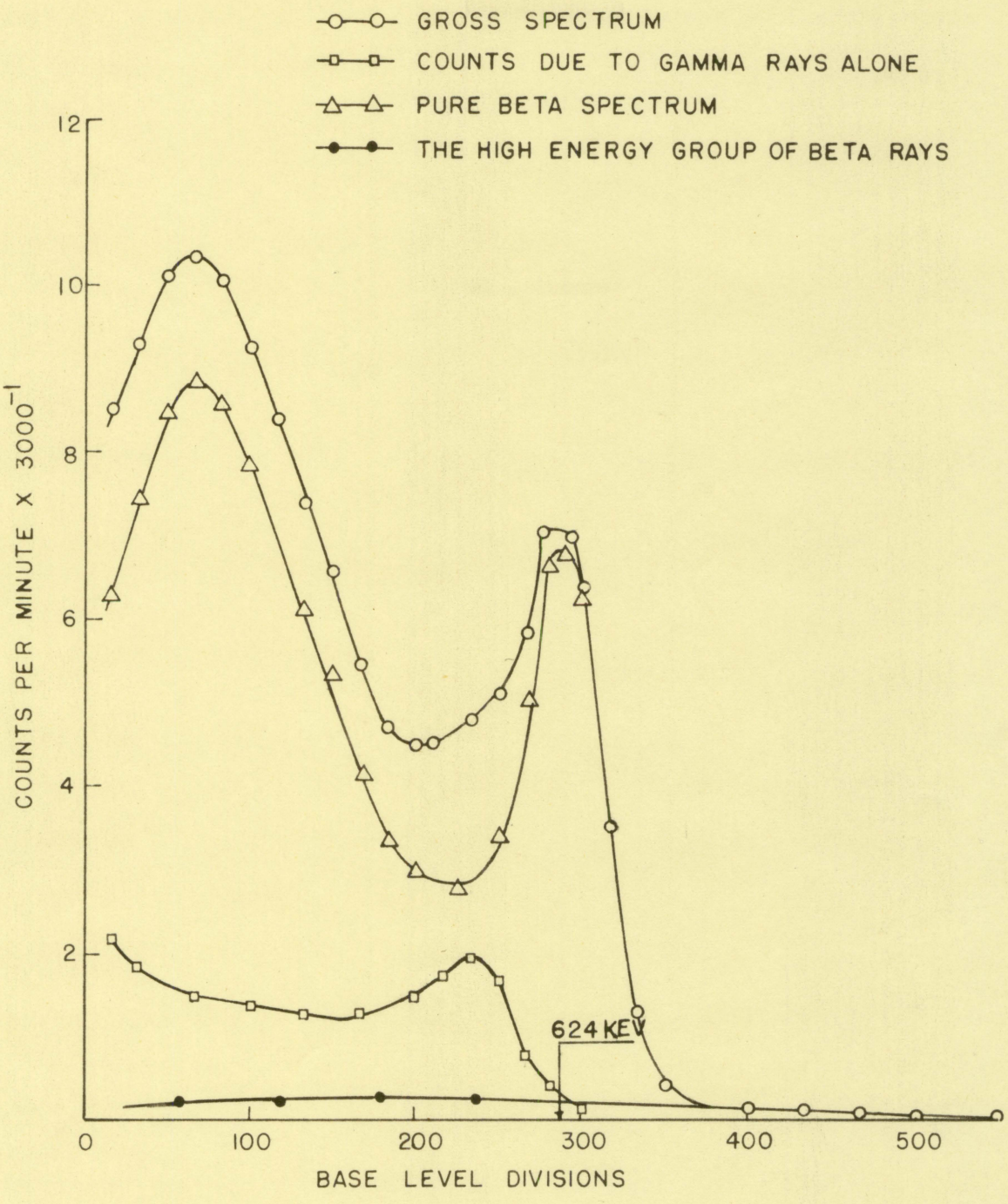

Figure 5. Experimental beta spectrum of Cs^{137}

down to the energy axis at the valley between the two peaks, but it is not found to be so. This effect was noticed also by Palmer and Laslett (11). This might be partly because some of the monoenergetic internal conversion electrons are scattered out of the crystal before all of their energy is absorbed in the phosphor and partly due to a high energy beta ray group of low abundance, which is shown to exist by Langer and Price (16). A Kurie plot of the spectrum is shown in Figure 6. The high energy component is extrapolated backwards as a straight line and by reverse calculations used in the Kurie plot, the distribution of the high energy component is separated. This is shown in Figure 5. From the net pure beta spectrum, this high energy distribution is subtracted and the Kurie plot of this low energy group spectrum is shown in Figure 6. This line can be extrapolated downwards giving an end point energy of 0.56 Mev. This is within an accuracy of 9 percent of the accepted value of 0.51 Mev. The higher energy group is found to have the end point at 1.33 Mev. There is a good chance of error due to graphical analysis in the results obtained.

From Figure 7 it is found that the distribution of the internal conversion peak is rather narrow with a half-width of only 61 base-level divisions at "Gain" 2. Obviously in the case of "Gain" 1, since the spectrum is almost halved in width, the peak is even narrower than for "Gain" 2. At "Gain" 4, the half-width of the peak was found to be

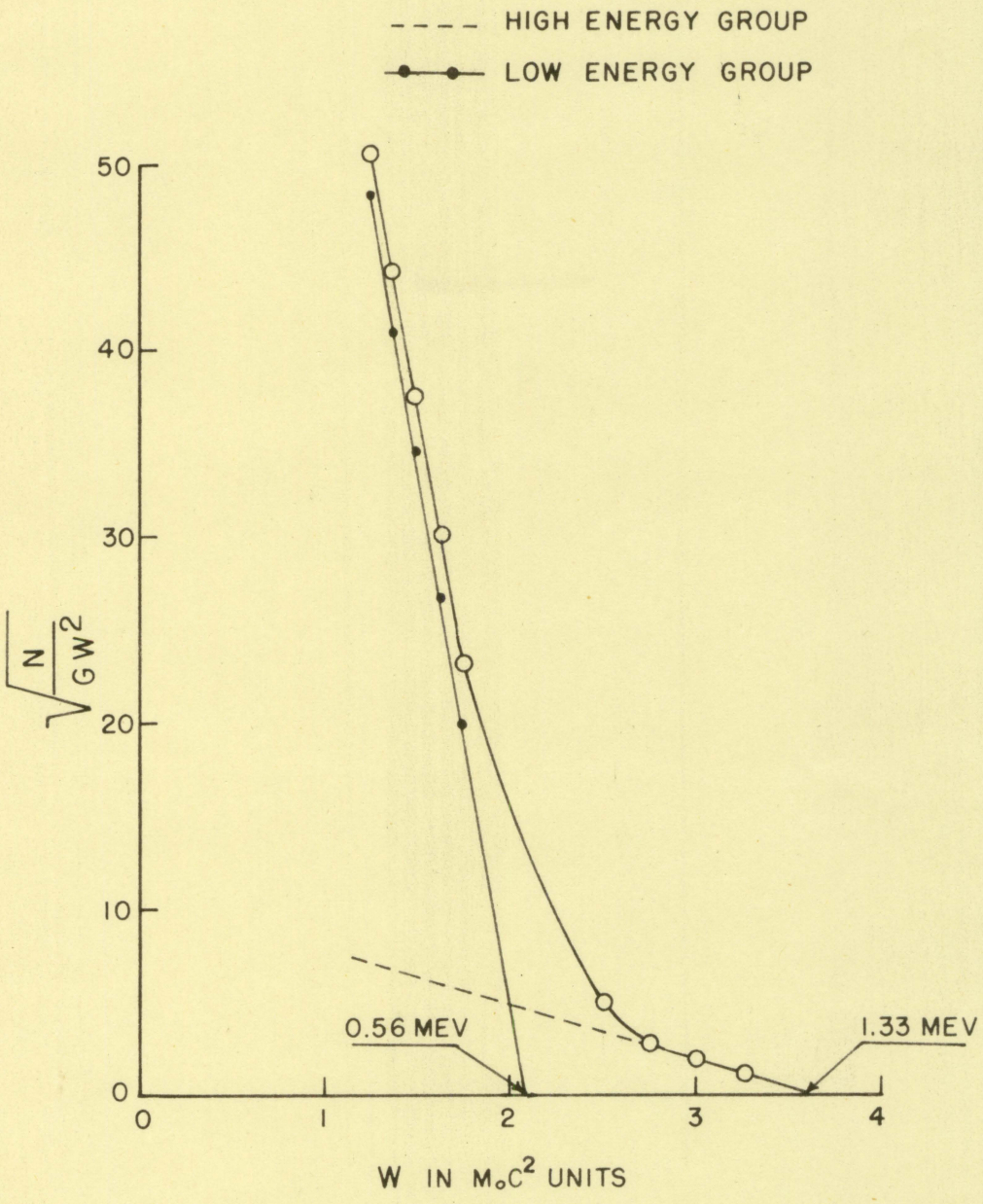

Figure 6. Kurie plot of the Cs^{137} spectrum

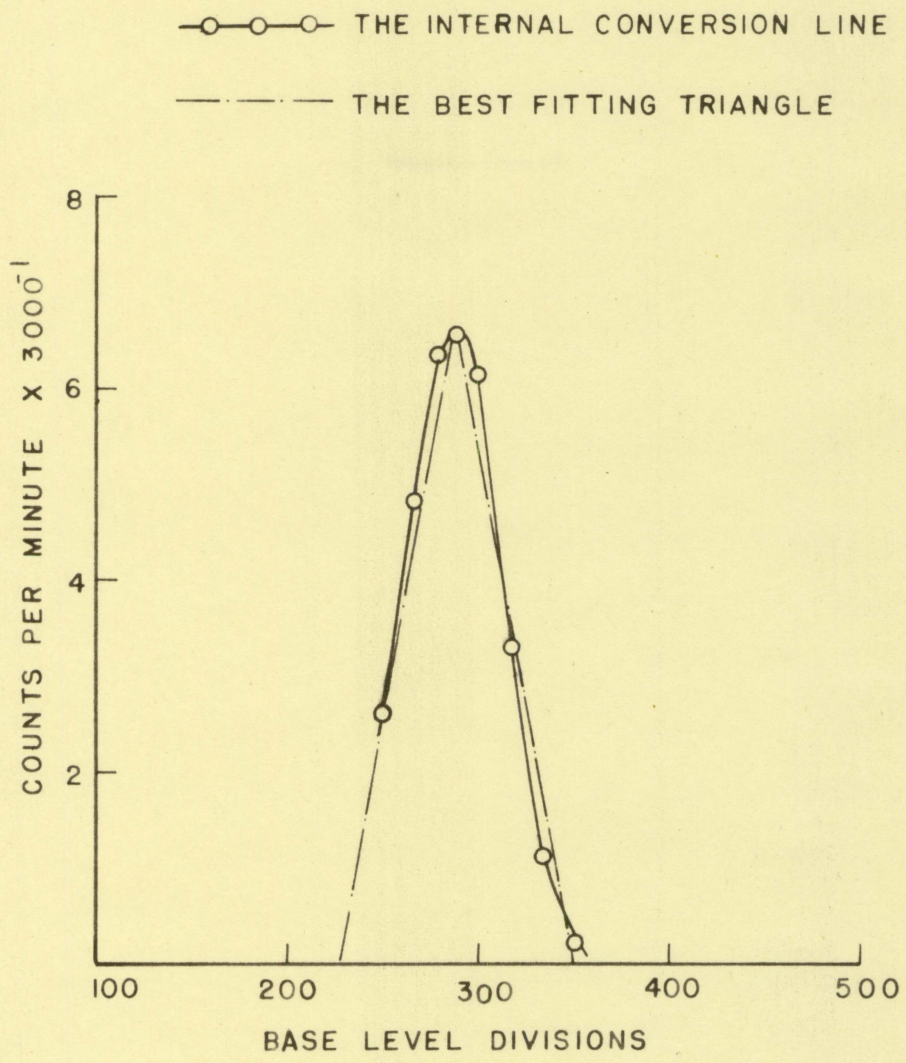

Figure 7. Internal conversion peak of Cs^{137} approximated by a triangle

129 minor divisions for stilbene. For anthracene, the half-widths were found to be almost 17 percent less than for stilbene. As we have seen in Section IV, transmission corrections depend on the half-width and so, for spectra recorded with "Gain" 1 and 2, transmission corrections are not of much effect. But for "Gain" 4, it will certainly have some effect on the end point of the spectrum. In this work almost all the spectra except that of Nd^{147} were taken at "Gain" less than 4 and so transmission corrections have not been applied.

C. Strontium-90 and Yttrium-90

The combined spectrum of Sr^{90}-Y^{90} mixture at secular equilibrium is shown in Figure 8, as recorded by the spectrometer, using a stilbene crystal.

The two components of the spectrum can be identified very clearly from the figure. A Kurie plot of the combined spectrum is shown in Figure 9. This plot is a straight line at high energies and then suddenly it shoots upward showing the presence of Strontium-90 beta rays. This straight line portion could be extrapolated and the Y^{90} spectrum could be separated from the combined spectrum as shown in the case of Cesium. But this would not give a true end point for Sr^{90} because of the possible curvature of the Kurie plot of the Y^{90} spectrum at low energies. This curvature, as explained earlier, is due to electrons being scattered out of

Figure 8. Strip-chart recording of the beta spectrum of Sr^{90}-Y^{90} mixture at secular equilibrium

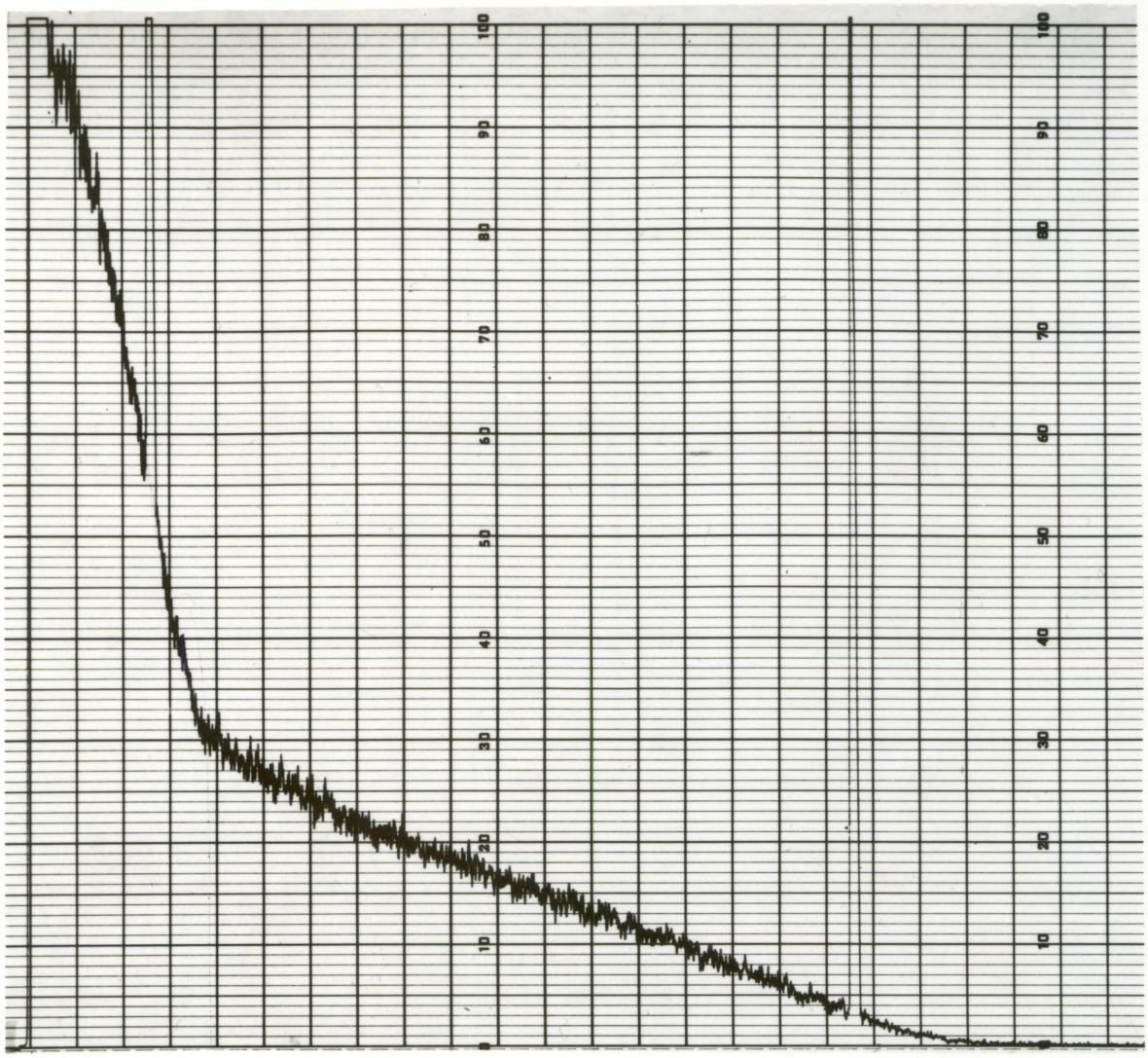
100
90
80
70
60
50
40
30
20
10
0

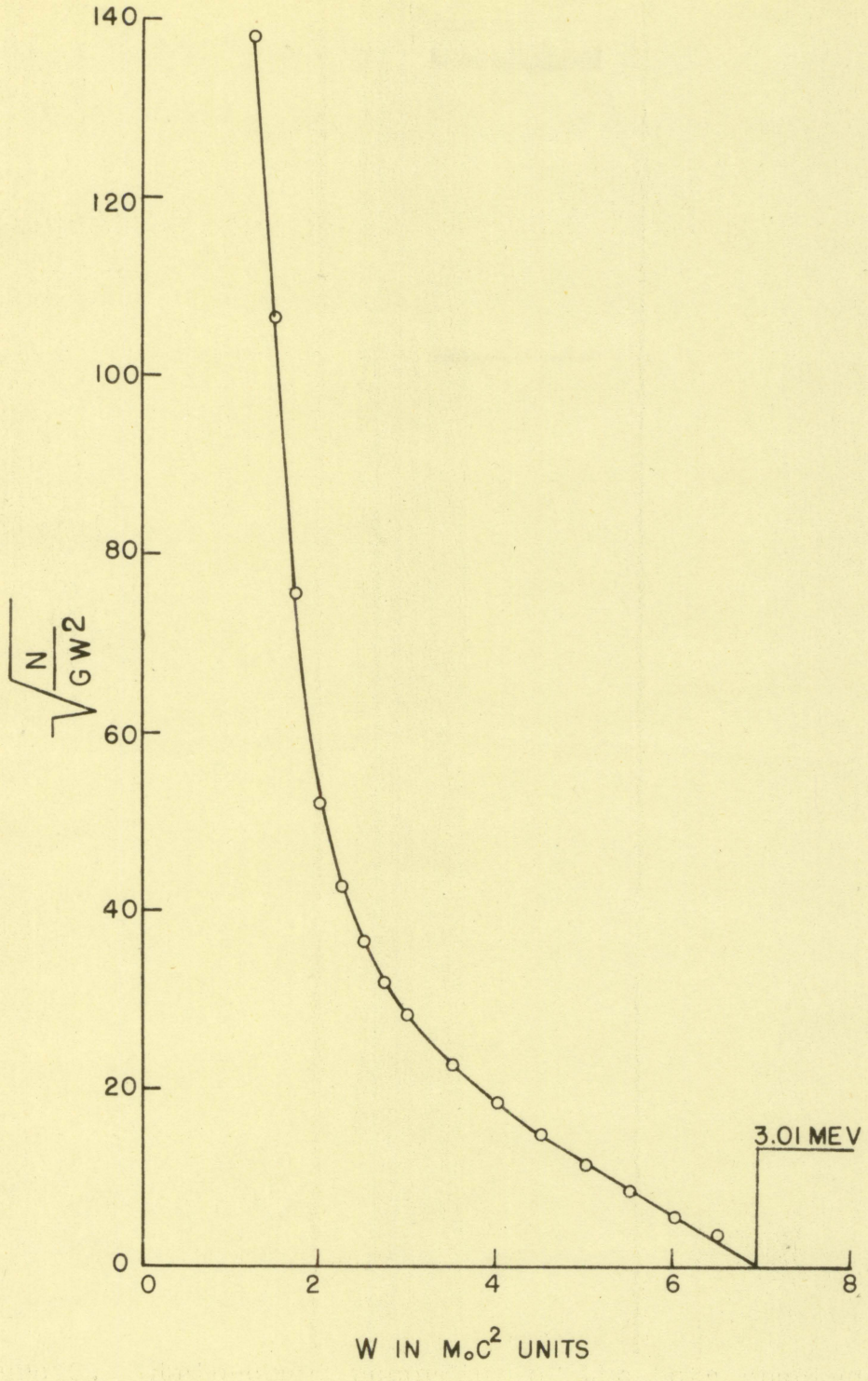

Figure 9. Kurie plot of the Sr^{90}-Y^{90} spectrum

the crystal before their energy is totally absorbed by the crystal, thereby increasing the number of low energy pulses.

The end-point energy is found to be 3.01 Mev. The accepted value is 2.28 Mev, for Y^{90}. So our result has an error of 24 percent which is too much to be attributed to the unavoidable experimental errors. It should be noticed that this spectrum was plotted at "Gain" 1 and the calibrating point was 624 Kev at 138 minor divisions on the base-level scale, which is only about $\frac{1}{6}$ of the base-level at the end point. So this error could easily have been caused by a slight variation in the assumed linearity of the energy calibration, as we were trying to calculate an energy which is about 4 times bigger than the calibration point.

Yttrium-90 was separated from Sr^{90} using the ion exchange separation and the spectrum of the Y^{90} sample obtained is shown in Figure 10. Figure 11 shows the Kurie plot of this spectrum. The quality of the resin used for the separation was not quite good and so the purity of the sample was questionable as can be noticed from the Kurie plot. However, this line is a little more straight than in the case of the combined spectrum. The end-point energy determination of this spectrum gives a value of 2.99 Mev and the error is therefore 23.7 percent. This is a slightly better value than for the first case.

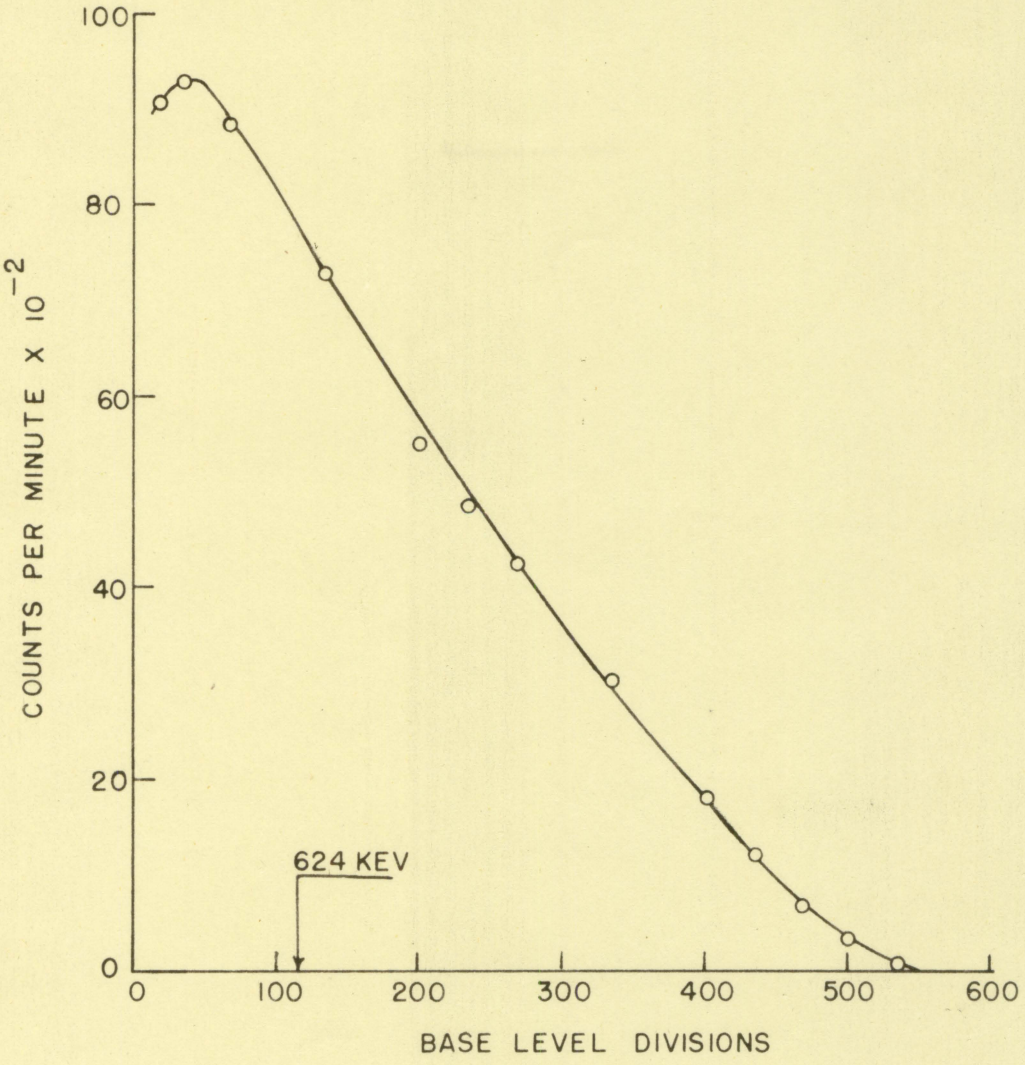

Figure 10. Experimental beta spectrum of Y^{90}

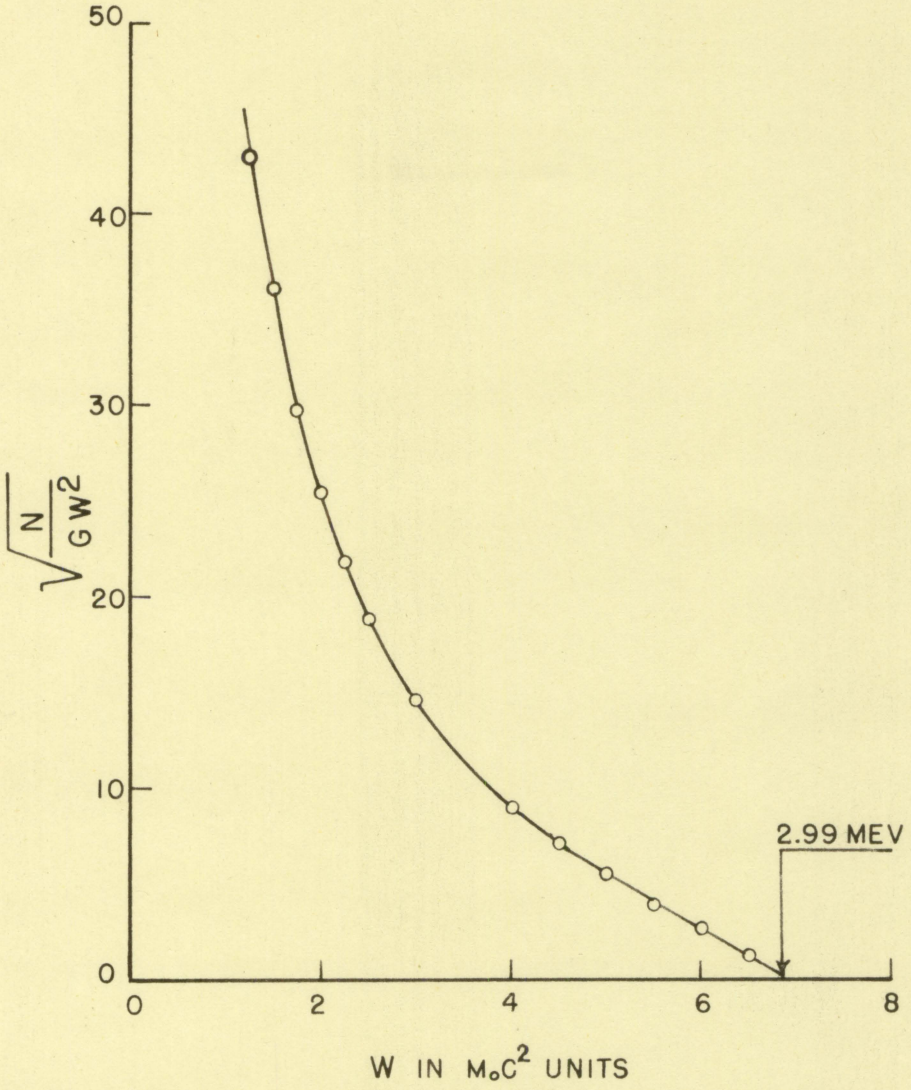

Figure 11. Kurie plot of the Y^{90} spectrum

D. Cerium-144 and Praseodymium-144

This is a well-known combination emitting beta rays and very weak gamma rays. The beta rays of Cerium-144 are rather insignificant when compared to those of Pr^{144}. This is quite clearly shown in the spectrum of the mixture at secular equilibrium, given in Figure 12. Just when the Pr^{144} spectrum was reaching its peak, the beta rays emitted by the Ce^{144} were added to it and the total spectrum is shifted steeply upwards.

A Kurie plot of this spectrum is shown in Figure 13. Here also, the presence of the Cerium component is quite conspicuous. Determination of the end-point energy leads to a value of 3.68 Mev as against the accepted value of 2.98 Mev. The percentage error is, therefore, about 19.

Only one main group of beta rays is emitted from Pr^{144} and normally there should be a clear breaking point in the Kurie plot where the Ce^{144} and Pr^{144} components join together. This is not found in Figure 13, only because of the low energy scattering of electrons emitted by Pr^{144}.

The contribution due to the gamma rays were not subtracted from the gross spectrum, since they are too weak even to get through the aluminum absorber which should be thick enough to absorb the high energy beta rays. Also, the contribution due to these gamma rays is quite negligible (19).

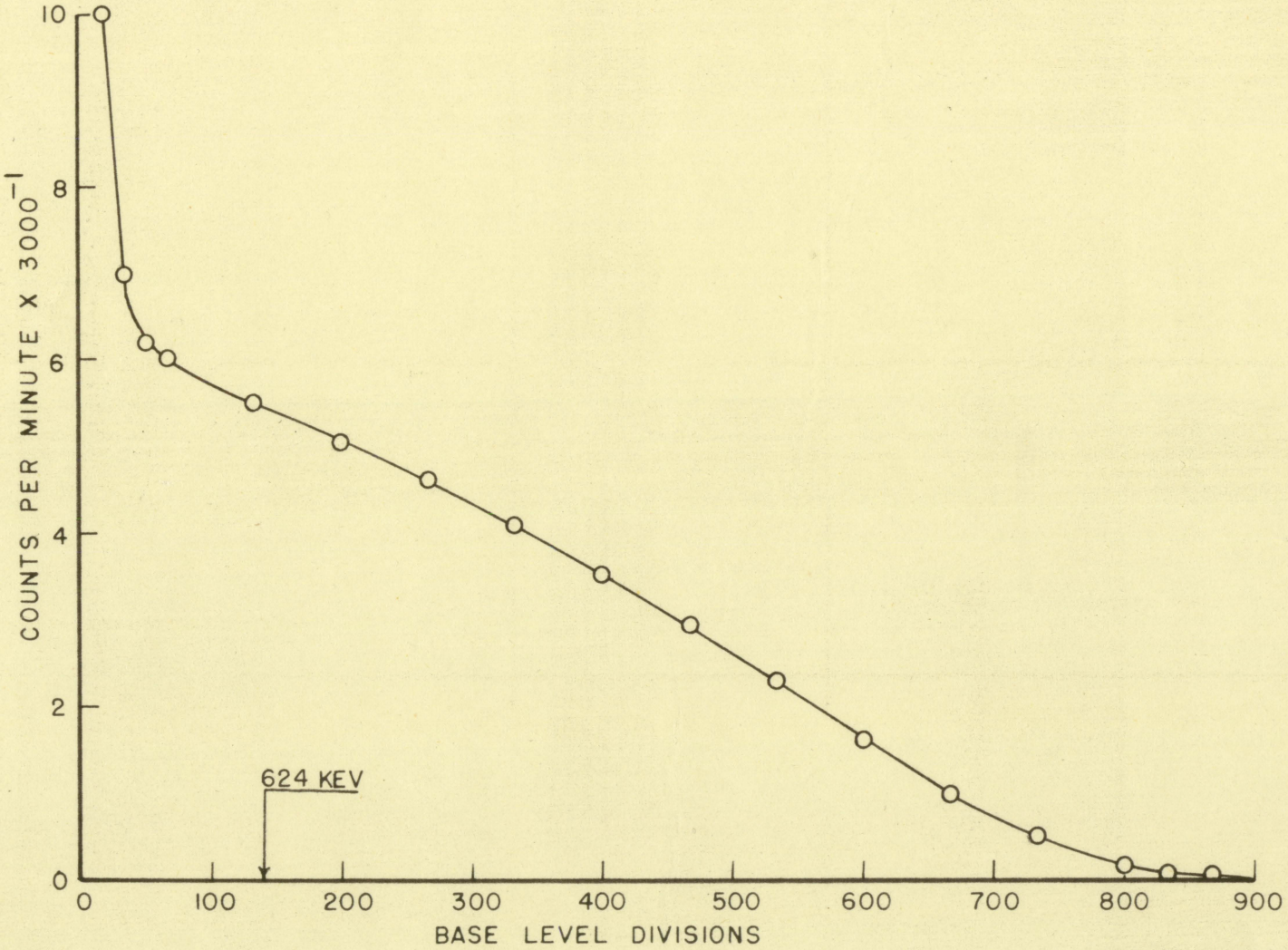

Figure 12. Experimental beta spectrum of Ce^{144}-Pr^{144} at secular equilibrium

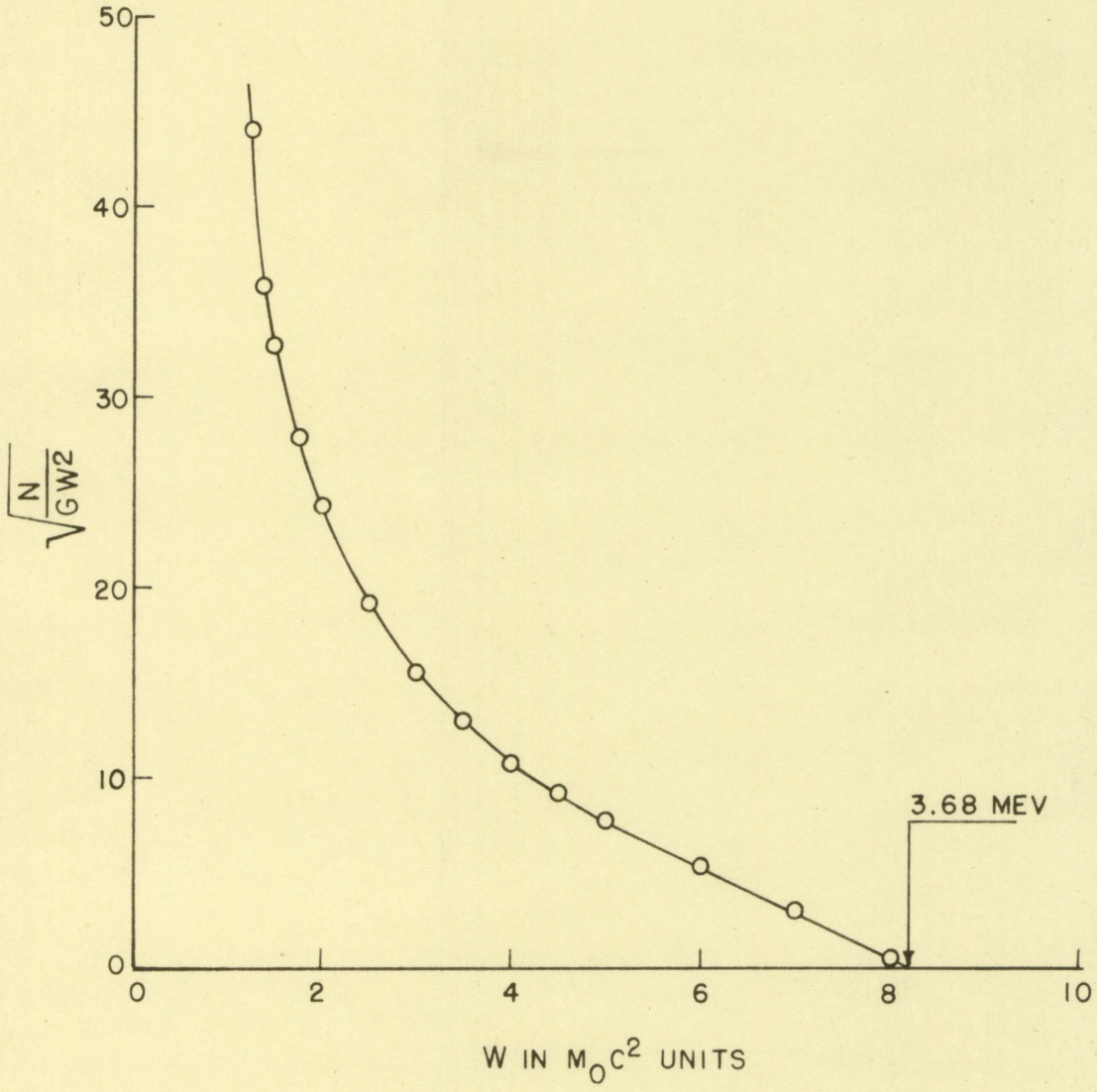

Figure 13. Kurie plot of the Ce^{144}-Pr^{144} spectrum

E. Ruthenium-106 and Rhodium-106

This combination is similar to the Cerium-Praseodymium mixture. Rh^{106} is known to have the most energetic beta rays among all the isotopes while the beta rays of Ru^{106} is relatively weak. Rh^{106} has a very complex disintegration scheme and gamma rays of different energies are also emitted.

The energy spectrum of the combination is shown in Figure 14. Its shape is different from that of the Ce^{144}-Pr^{144} spectrum in the respect that, in the case of Ruthenium and Rhodium, the contribution by Ru^{106} is relatively very small and so the gross spectrum has a narrow peak at very low energies.

The effect of gamma rays was eliminated by using suitable aluminum absorber and then subtracting the gamma counts from the gross counts. Figure 15 shows the Kurie plot. The curvature is due to three main reasons. First of all, there are many groups of beta rays of different energy in the Rh^{106} component. Secondly, the incomplete absorption of energy in the crystal due to scattering of electrons increases the number of counts at low energies. Thirdly, the Ru^{106} beta rays make some finite contribution. But, it is very hard to say which one of these makes the most predominant contribution to low energy pulses.

The end-point energy determination from the Kurie plot gives a value of 4.47 Mev for the Rh^{106} component. This

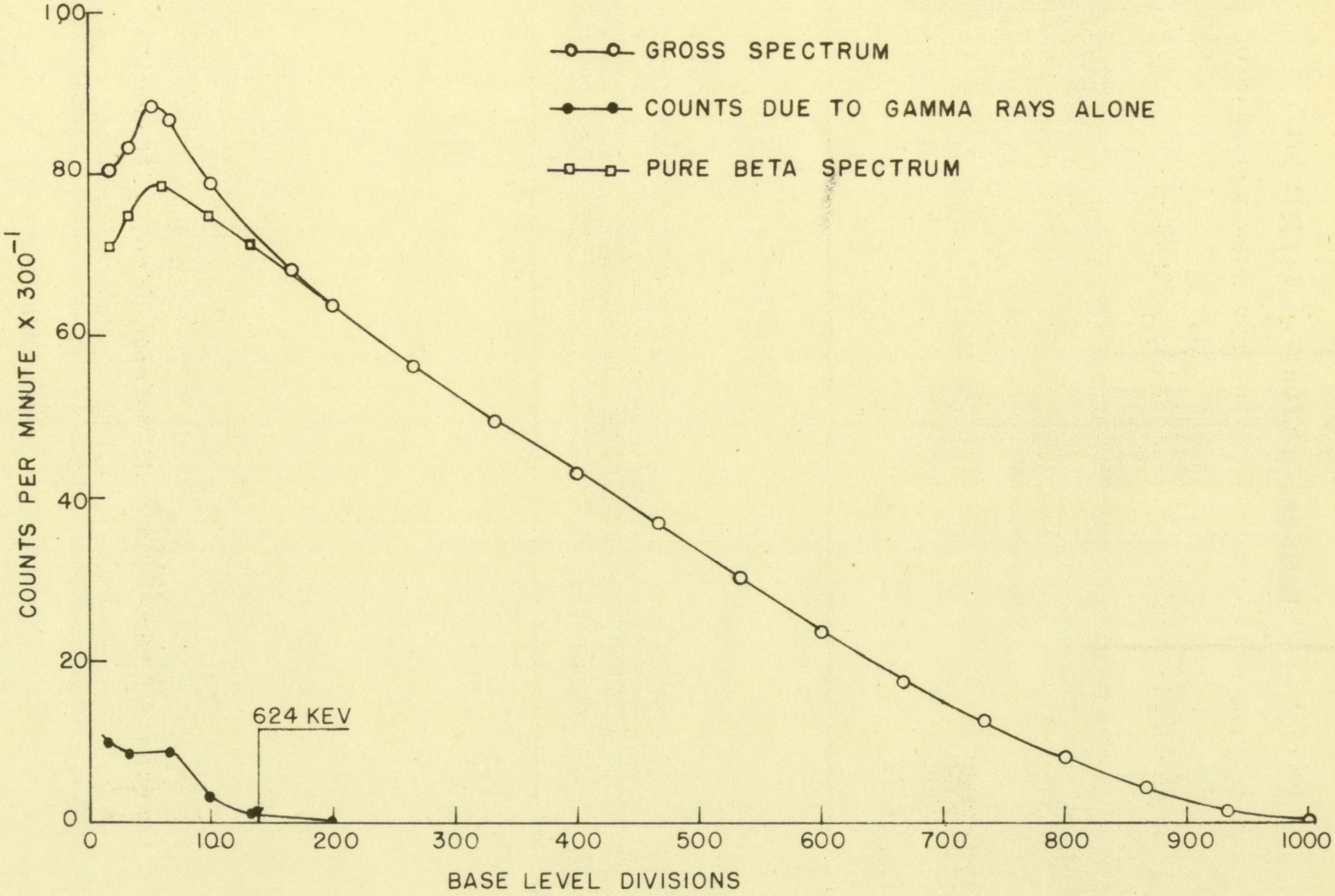

Figure 14. Experimental beta spectrum of Ru^{106}-Rh^{106} at secular equilibrium

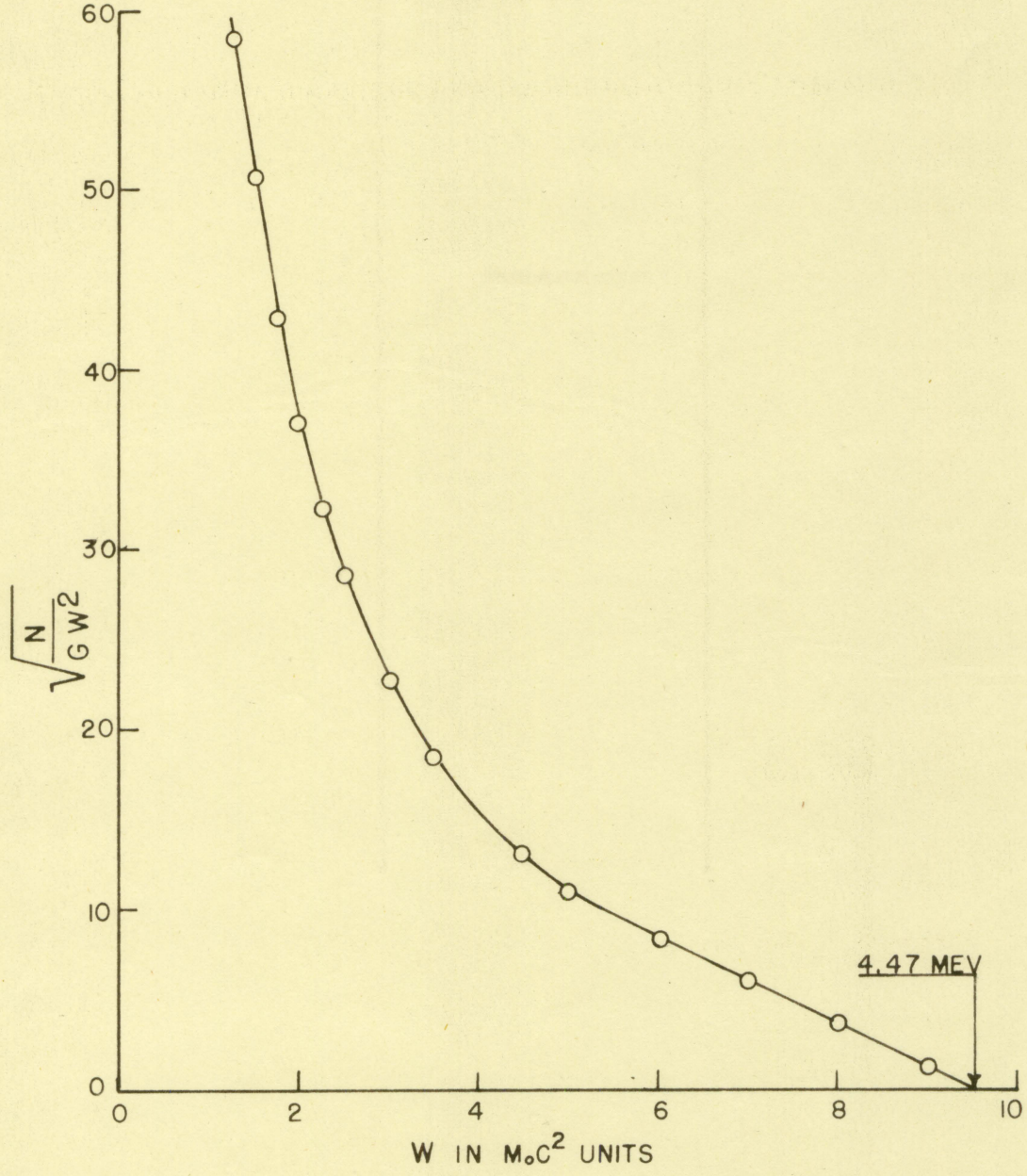

Figure 15. Kurie plot of the Ru^{106}-Rh^{106} spectrum

deviates by an error of 21 percent from the accepted correct value of 3.53 Mev. But it must be noted that the ratio of the correct end-point energy to the energy at calibration point, in this case, is 5.7.

F. Neodymium-147

Neodymium-147 also has a complex disintegration scheme and it emits beta rays of moderate energy and also gamma rays.

The gross spectrum and also the gamma subtracted spectrum are shown in Figure 16. Figure 17 gives the Kurie plot of this spectrum. Although the spectrum is known to be complex (20), the Kurie plot is found to be almost a straight line. Two points can be inferred from this fact. First of all there is not a wide difference between the maximum energies of the several groups of beta rays, unlike the cases of Sr^{90}-Y^{90}, Ru^{106}-Rh^{106}, and Ce^{144}-Pr^{144} combinations. Secondly, the group which has the highest energy has the highest abundance also.

The end-point energy is found to be 0.94 Mev from the Kurie plot. This deviates by about 13 percent from the accepted value of 0.82 Mev. This spectrum was recorded at "Gain" equal to 4 and so transmission corrections could be applied to it. This might reduce the error in the end point energy to some extent, but the change in the end-point energy will not be very much.

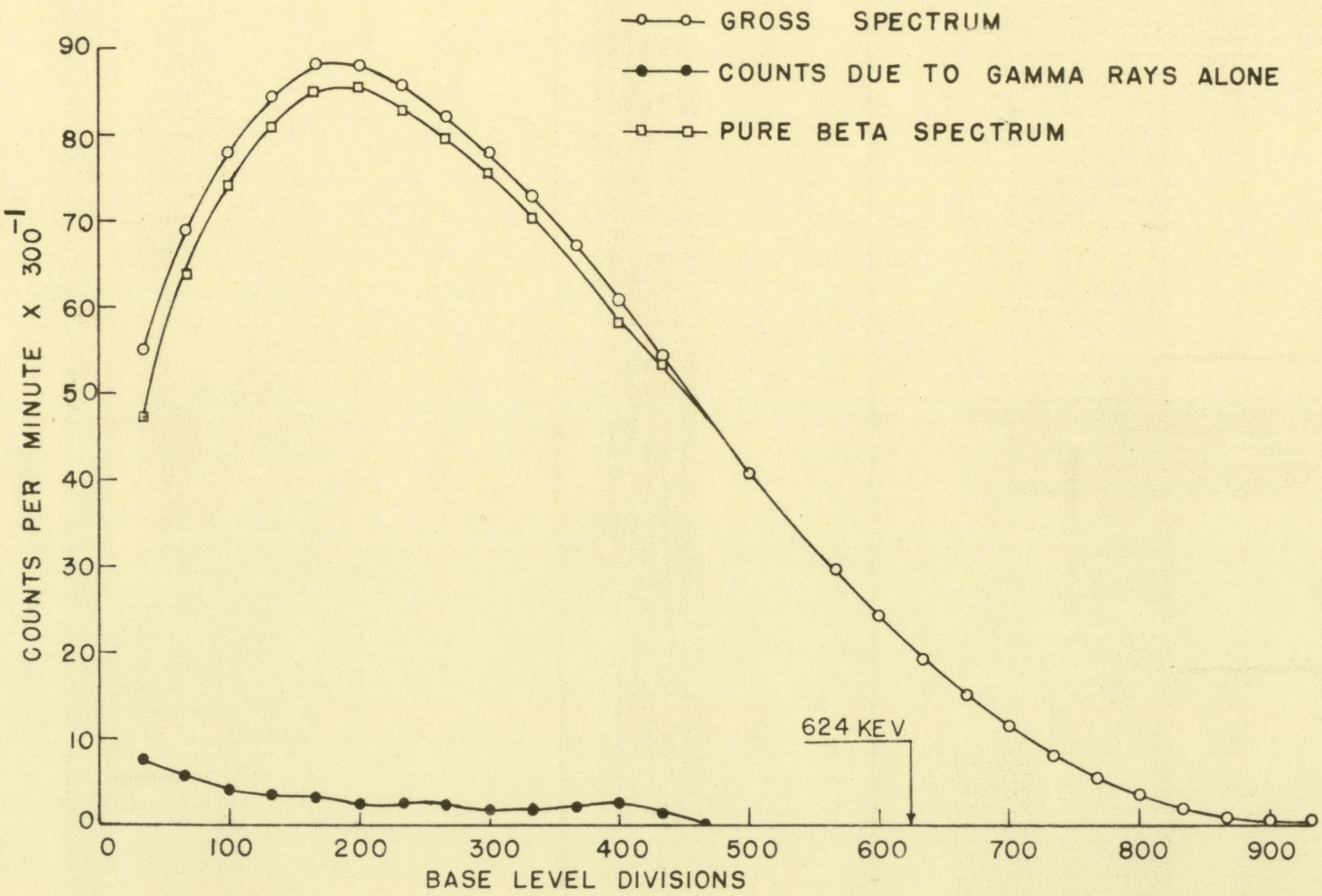

Figure 16. Experimental beta spectrum of Nd^{147}

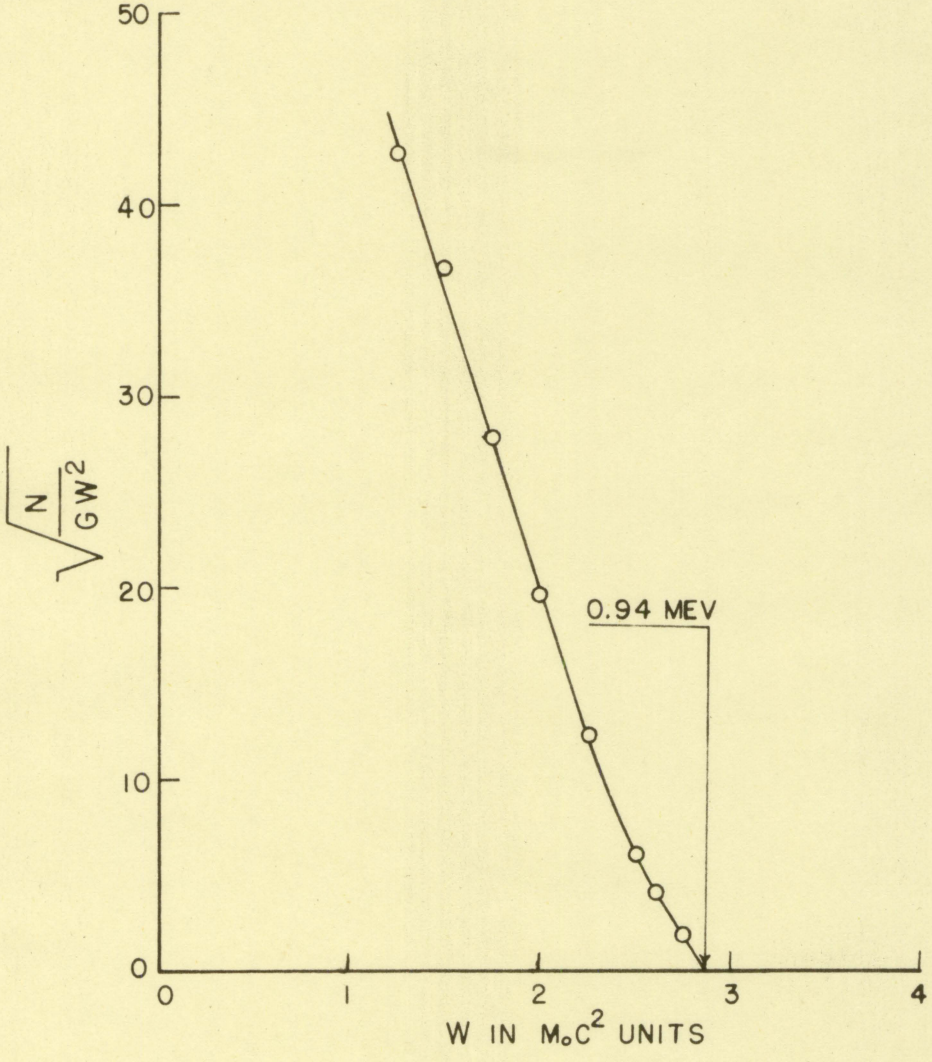

Figure 17. Kurie plot of the Nd^{147} spectrum

VI. CONCLUSIONS

From the results discussed in Section V, it is very clear that the accuracy that can be obtained with this commercial equipment depends on the energy we want to measure. Below 2 Mev, reasonable accuracy can be obtained. But when higher energies are to be measured, the calibration of the instrument has to be done very carefully. Figure 18 shows a plot of the variation of the observed energy with the true energy, as obtained from the results of this investigation.

The experimental accuracy of this work is questionable, because of the relatively low energy of the calibration point, vis., the 624 Kev, internal conversion peak of Cs^{137}, when compared to the magnitude of the energies that were measured.

A better method for the calibration of this instrument would be to take two or three calibration points instead of one, in the range of the energies to be measured and then assume linear variation between these points. The internal conversion peaks of Cobalt-60 could be ideal calibration points mainly because of their high energies, 1.16 Mev and 1.32 Mev.

The scattering of electrons from the crystal causes some inaccuracy and it also complicates the analysis of the spectrum. Perhaps by knowing the true response at low energies when the instrument is used to analyze monoenergetic electrons

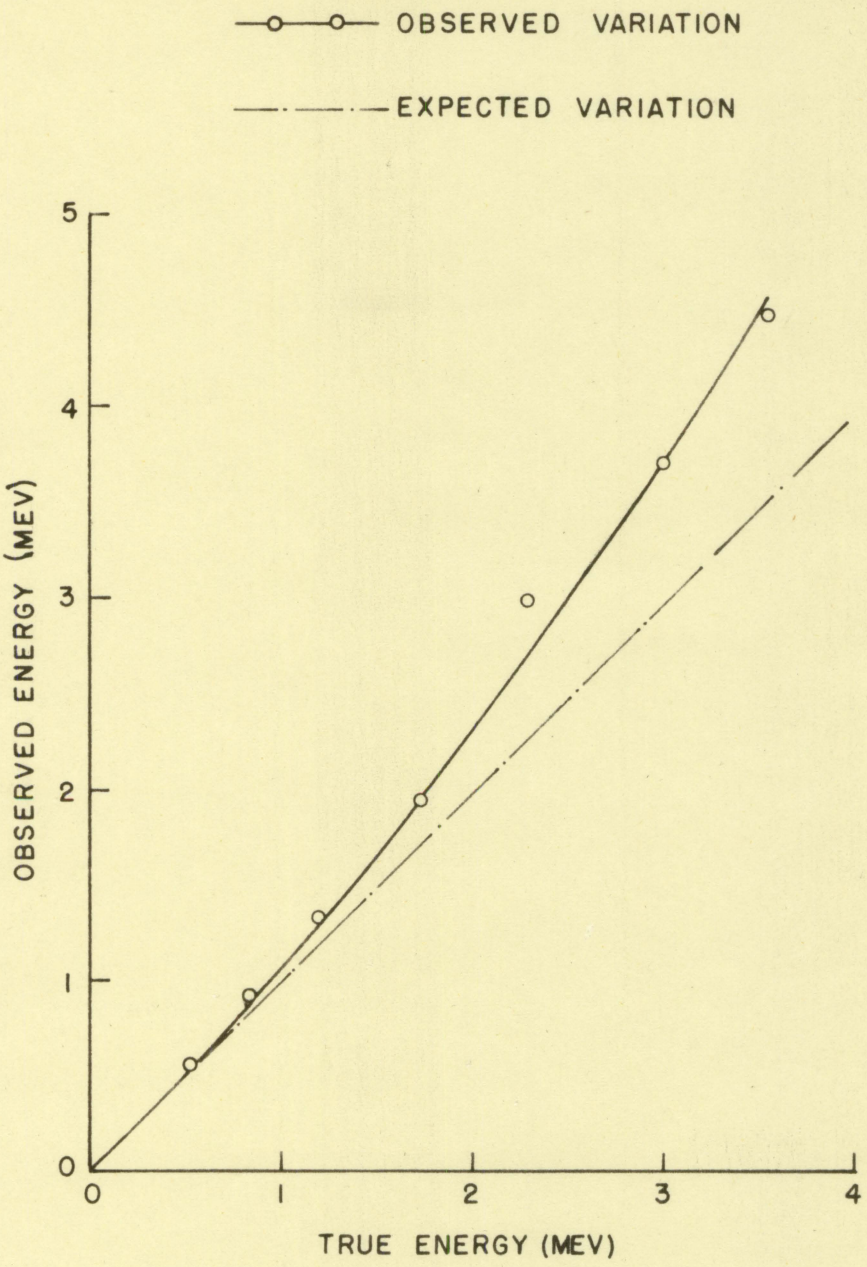

Figure 18. Experimental variation in the energy calibration

a correction could be applied to the scattering effect. Also, this could be further improved by using a better geometrical arrangement of the scintillation detecting unit, as for example the split-crystal technique.

This instrument is found useful when the spectrum is to be recorded in the quickest way possible at the expense of precision. It is also useful in investigating the activities of low energy beta radiation in which case the magnetic spectrometer becomes very complicated.

VII. LITERATURE CITED

1. Curran, S.C. Luminescence and the scintillation counter. New York, Academic Press Inc., Publishers. 1953.

2. Kallman, H. Luminescent counters. London Research 2: 62-68. 1949.

3. Coltman, J.W. and F.H. Marshall. Some characteristics of the photo-multiplier radiation detector. Physics Review 72: 528. 1947.

4. Deutsch, M. Scintillation counters with naphthalene. Massachussets Institute of Technology Laboratory for Nuclear Science and Engineering. Technical Report No. 3. September 1, 1947.

5. Bell, P.R. The use of anthracene as a scintillation counter. Physics Review 73: 1405. 1948.

6. Hopkins, J.I. The response of the anthracene scintillation counter to monoenergetic electrons. Physics Review 77: 406. 1950.

7. Morton, G.A. Photomultipliers for scintillation counting. R.C.A. [Radio Corporation of America] Review 10: 525-552. 1949.

8. Jordan, W.H. and P.R. Bell. Scintillation counters. Nucleonics 5, No. 5: 30-41. October, 1949.

9. Bell, P.R. The scintillation method. In Siegbahn, K., ed. Beta- and gamma-ray spectroscopy. pp. 132-164. New York, Interscience Publishers, Inc. 1955.

10. Ketelle, B.H. The Ca^{45} beta-distribution obtained in a split-crystal scintillation spectrometer. Physics Review, Ser. 2, 80: 758. 1950.

11. Palmer, J.P. and L.J. Laslett. Application of scintillation counters to beta-ray spectroscopy. U.S. Atomic Energy Commission Report ISC-174 [Iowa State Coll., Ames]. December, 1950.

12. Sangster, R.C. A study of organic scintillators. Massachussets Institute of Technology Laboratory for Nuclear Science and Engineering. Technical Report No. 55. December 1, 1952.

13. Morton, G.A. and J.A. Mitchell. Performance of 931-A type multiplier as a scintillation counter. Nucleonics 4, No. 1: 16-23. 1949.

14. Rose, M.E., N. M. Dismuke, C.L. Perry and P.R. Bell. Tables of Fermi Functions. In Siegbahn, K., ed. Beta- and gamma-ray spectroscopy. pp. 875-879. New York, Interscience Publishers, Inc. 1955.

15. Langer, L.M. and H.C. Price, Jr. Forbidden spectra of Sr^{89}-Y^{90}. Physics Review 76: 454. 1949.

16. Langer, L.M. and H.C. Price, Jr. Beta spectra of forbidden transitions. Physics Review 76: 641. 1949.

17. Mitchell, A.C.G. and H. Slatis. -spectrometer measurements (1). In Siegbahn, K., ed. Beta- and gamma-ray spectroscopy. pp. 224-258. New York, Interscience Publishers, Inc. 1955.

18. Wapstra, A.H., G.J. Nijgh and R. Van Lieshout. Nuclear spectroscopy tables. Amsterdam, North Holland Publishing Company. 1959.

19. Ajzenberg-selove, F. Nuclear spectroscopy. Part A. New York, Academic Press, Inc., 1960.

20. Strominger, D., J.M. Hollander and G.T. Seaborg. Table of isotopes. Reviews of Modern Physics 30, Part 2: 585. 1958.

VIII. ACKNOWLEDGMENTS

It is with great pleasure that I express my sincere appreciation to Dr. A. F. Voigt for suggesting this research topic and for his valuable suggestions and guidance throughout the progress of this investigation. I am also indebted to Dr. Glenn Murphy for his thorough cooperation in this programme. My sincere thanks also go to Mr. Melvin Foster of the Chemistry department for his suggestions and encouragement and also for the interest he showed during the time of the experimental work. Mr. Kenneth Malaby of Ames Laboratory was kind enough to prepare some radioactive samples for use in this investigation and I express my sincere thanks to Mr. Malaby.

IX. SUPPLEMENT

As shown in Section VI, since the variation of energy with the base level scan is not linear, it is evident that calibration is not possible using a single calibration point. It is worthwhile to investigate the possibility of calibrating the instrument using some known beta ray end-point energies.

A check on this method can be made using the experimental data we already have. The 624 Kev internal conversion line of Cs^{137}, the 1.71 Mev end-point of P^{32} and the 3.53 Mev end-point of Rh^{106} are used for this purpose. A calibration curve between the observed maximum energies of these three isotopes and their actual maximum energies is plotted and this curve is shown in Figure 19. Using this curve, the Kurie plots of the other isotopes can be corrected and the end-point energies can be redetermined. As expected, the accuracy in the determination of end-point energies is very much improved by this method of calibration. Table 2 gives the results obtained. Using these results, the curve shown in Figure 18 is replotted and is shown in Figure 19 as the curve of observed variation of energy.

The error observed in the results obtained using single point calibration was almost halved in this case. Also, the Kurie plots were found to be straighter than in the previous case. Even with this correction, the error in the case of Sr^{90}-Y^{90} is considerably high. A plausible reason for this

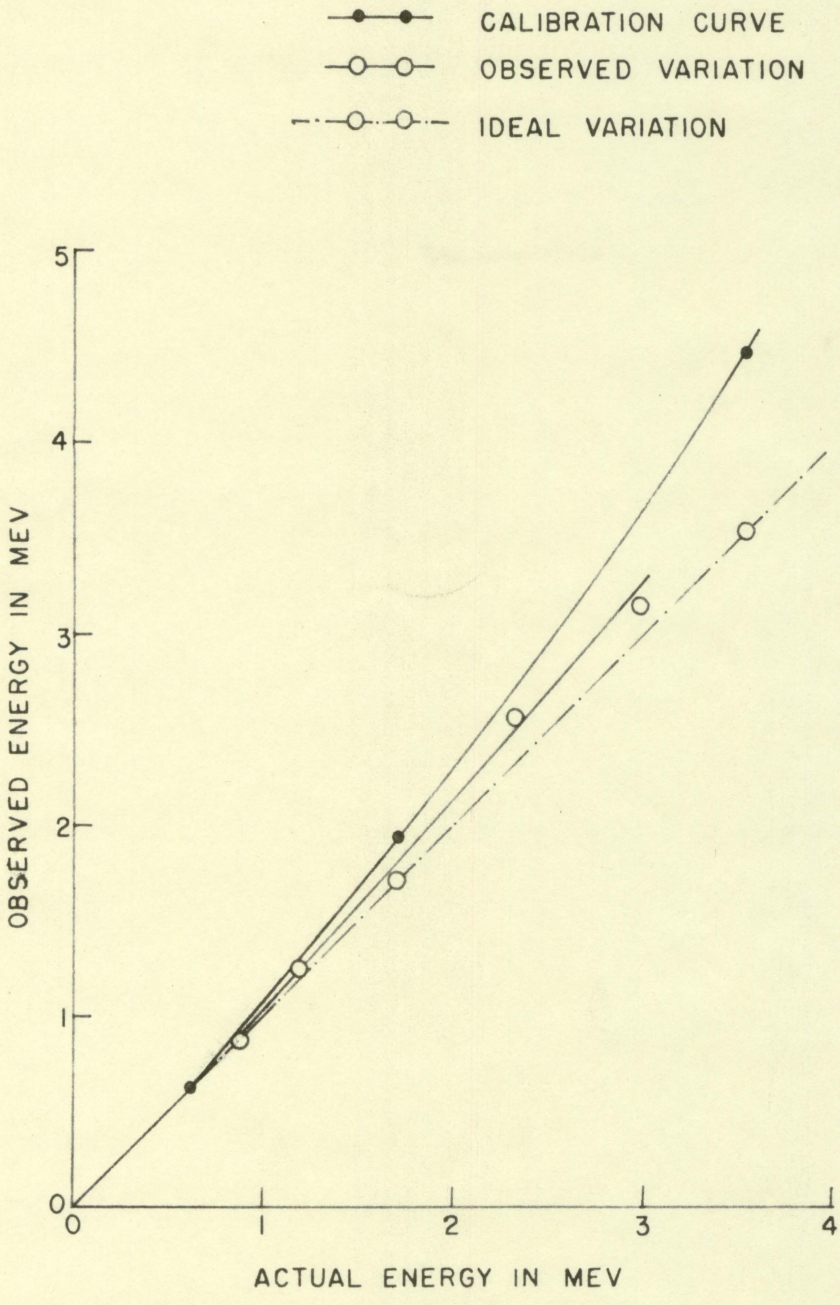

Figure 19. Calibration curve and experimental variation in energy calibration

can only be some inherent mistake in the treatment of the distribution of beta particles emitted by these isotopes. However, considering the accuracy obtained in the case of the other isotopes, it can be concluded that the best way to calibrate this spectrometer for experimental purposes is by using isotopes with well-known end-point energies.

Table 2. End-point energies and percentage errors

Isotope	Maximum energy of beta decay in Mev	Percentage error
Cs^{137}	1.25	4.8
Sr^{90}-Y^{90}	2.65	14.0
Y^{90}	2.56	11.0
Ce^{144}-Pr^{144}	3.15	5.3
Nd^{147}	0.88	6.8